Geochimica et Cosmochimica Acta Vol. 54, pp. 2657–2677

0016-7037/90/$3.00 + .00

A new kinetic approach to modeling water-rock interaction: The role of nucleation, precursors, and Ostwald ripening

CARL I. STEEFEL and PHILIPPE VAN CAPPELLEN
Department of Geology and Geophysics, PO Box 6666, Yale University, New Haven, CT 06511, USA

(*Received January* 29, 1990; *accepted in revised form July* 20, 1990)

Abstract—A new approach to water-rock interaction is developed which replaces the assumption of partial equilibrium with a complete calculation of the rates at which minerals form and dissolve. The evolution of reaction-flow systems towards equilibrium with respect to secondary phases is examined in terms of the important processes which generate and modify reactive surface areas of minerals: heterogeneous nucleation, crystal growth, dissolution, and crystal ripening. The widespread occurrence in surficial environments of metastable solid phases and waters supersaturated with the thermodynamically most stable minerals is attributed to the slow rates of reactive surface area generation of the latter. This is primarily because the high mineral-solution interfacial tensions of the stable minerals make it difficult to nucleate them directly. In many cases, a stable mineral circumvents direct nucleation by using as a template for its own growth a more soluble, metastable precursor. Continued growth will ultimately bring the solution composition towards equilibrium with respect to the stable secondary mineral. The common persistence of the precursor and/or intermediate phases halloysite and allophane in weathering profiles indicates that geologically significant periods of time may be required to achieve equilibrium with kaolinite.

The reactive flow model presented explicitly calculates reactive surface areas of secondary minerals using crystal size distributions. The model includes rate expressions for heterogeneous nucleation, growth/dissolution, and Ostwald ripening along with an expression describing the competition of a stable mineral and its precursor for the available growth sites at the precursor's surface. The model is used to simulate the weathering of a fresh granite by infiltrating rain water. The simulations provide a semi-quantitative picture of how a reaction front develops in time and space.

INTRODUCTION

WATER-ROCK REACTIONS are driven by the influx of waters which are out of equilibrium with the mineral assemblage in the rock. This may cause, for example, the dissolution of primary minerals and lead to the build-up of supersaturation with respect to secondary minerals. The result is that, as the fluid moves along a flow path, its composition changes, ultimately evolving towards equilibrium with the primary mineral assemblage while a series of secondary minerals precipitate. It is the ultimate goal of water-rock modeling to be able to describe quantitatively the evolution of both the fluid composition and rock mineralogy in time and space.

The first models to consider water-rock interaction as a system of coupled dissolution and precipitation reactions were developed by Helgeson and coworkers (e.g., HELGESON, 1968; HELGESON et al., 1969). In these models, dissolution reactions of primary minerals are treated as irreversible processes, while equilibrium with respect to the secondary phases is assumed (partial equilibrium). In the classic case of chemical weathering of a granite discussed by HELGESON et al. (1969), for instance, an infiltrating rain water initially begins in the stability field of gibbsite; its composition then proceeds into the field of kaolinite and muscovite, before reaching equilibrium with primary K-feldspar. In other words, the evolution of the system is described by a single reaction path of the fluid through composition space. This translates along a flow path into a succession of zones of secondary minerals (gibbsite→kaolinite→muscovite), finally leading into fresh rock.

As stated clearly by HELGESON (1979), the assumption of partial equilibrium is only justified where the rate of precipitation of a secondary phase is faster than the rate of dissolution of the primary mineral(s). Stable, insoluble minerals, however, may be characterized by slow precipitation kinetics, even on geological time scales. Models like PATH (HELGESON, 1968) and early versions of EQ3/EQ6 (WOLERY, 1979) generally deal with a mineral with sluggish precipitation kinetics by simply eliminating it. An example is the frequent omission of quartz as a potential secondary mineral, and its replacement by thermodynamically less stable amorphous silica, for which partial equilibrium is then assumed. There are two main objections to this kind of approach. First, one has to make an *a priori* choice of the secondary minerals which are permitted to crystallize in the system. Second, no mechanism is provided for the more stable minerals to form, and the system may, for example, indefinitely remain supersaturated with respect to quartz. In other words, the models yield no information on the time-scale over which the system ages as the metastable phases are replaced by their more stable counterparts. This aspect of the evolution of water-rock systems has been relatively neglected in geochemistry (GARRELS, 1982).

The precipitation of a more soluble and less stable phase and its replacement by a series of progressively more stable phases is known as the *Ostwald Step Rule* (or *Law of Stages*). The explanation for this behavior lies in the kinetics of the precipitation process (DUNNING, 1969). The system preferentially forms the phase with the fastest precipitation rate under the prevailing conditions. The nucleation of a more soluble phase is kinetically favored over that of a less soluble analogue because the more soluble phase has the lower min-

eral-solution interfacial energy. Hence, when the supersaturation of the solution is sufficiently elevated, the metastable mineral may have the higher rate of precipitation. This explains the frequently observed formation of metastable aluminosilicates in weathering profiles. As the solution composition evolves, however, the relative rates of precipitation and dissolution will change, gradually resulting in the formation of more stable secondary mineral assemblages.

In this paper, we have adopted a kinetic formulation for describing the dissolution and precipitation processes in water-rock systems. The assumption of partial equilibrium is replaced by a complete calculation of the rates at which minerals form and dissolve. Whether or not a given phase appears in the system depends only on its rate of precipitation relative to that of the other minerals.

The reactive surface area is a critical parameter controlling the overall rate at which a mineral precipitates or dissolves. Reactive surface area is generated by nucleation and crystal growth and it is modified by dissolution and Ostwald ripening. We review and derive where necessary kinetic expressions describing these processes. As a mathematical tool for keeping track of the evolution of a mineral's reactive surface area and volume fraction, we introduce the crystal size distribution of the mineral and discuss how it can be calculated. The kinetic expressions are incorporated into a numerical reactive flow computer code which allows the coupling of the chemical reactions to the advective and dispersive transport of dissolved components. The model is then applied to weathering of a fresh granite, with an emphasis on the formation of halloysite as a metastable precursor to kaolinite.

REACTION-FLOW SYSTEMS

Reaction-flow systems are characterized by feedback between the mineral assemblage in the rock and the fluid composition. In response to the influx of reactive fluids, the mineral assemblage at any point in space changes with time as a result of dissolution and precipitation (Fig. 1). These mineralogical changes, in turn, exert a control on the fluid composition through the water-rock reactions which take place as the fluid moves down the flow path (i.e., the reactions may partly or completely buffer the solution composition). Because transport and reaction are coupled, mass transfer at any point in a reaction-flow system is influenced by the reactions taking place elsewhere in the flowfield.

The coupling of reaction and transport in reactive flow systems has several important implications. First, in the case where either the dissolution or precipitation reactions are slow, the possibility arises that the fluid may not equilibrate completely with the mineral assemblages in the rock over any given distance along the flowpath (LASAGA, 1984; LICHTNER, 1988a; KNAPP, 1989; STEEFEL and LASAGA, 1990). In other words, the characteristic time for a fluid to achieve equilibrium with a mineral assemblage must be compared with the characteristic time required for the aqueous species to be transported some distance through the rock. When the time scale for equilibration is smaller than the transport time *given some length scale of interest*, then the *local equilibrium* condition holds. In many cases, however, reaction rates will not be fast enough relative to the transport rates, and local disequilibrium will result (STEEFEL and LASAGA, 1990; NAGY et al., 1990).

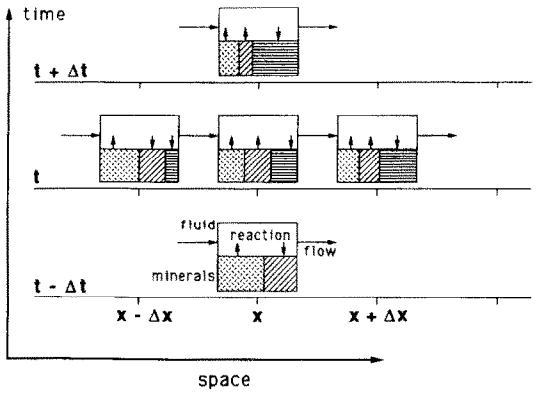

FIG. 1. Schematic representation of the finite difference approach for reaction-transport modeling. At each grid point along a flowline, a set of differential equations conserving the masses of the chemical components in the system is solved, taking into account transport (advection and dispersion) and reaction (homogeneous and heterogeneous) (see Appendix I). Heterogeneous mineral-water reactions are included in the model using finite precipitation-dissolution rates which depend on both the solution composition and the reactive surface areas of the minerals. This formulation provides for feedback between mineral assemblage and fluid composition. In response to the constant influx of reactive fluid, the mineral assemblage at any given grid point evolves with time. The fluid, in turn, is modified because of the differing mineral assemblages it encounters as it moves down a flowpath. Because transport and reaction are coupled, mass transfer at any point in the system is influenced by reaction taking place elsewhere in the flowfield.

In the example of granite weathering discussed by HELGESON et al. (1969), the assumption of partial equilibrium with respect to the secondary minerals and the presence throughout the simulation of the primary, irreversibly reacting mineral (feldspar, in that example) guarantees that a single reaction path describes the chemical evolution of the fluid. Where either the mineral dissolution or precipitation rates are slow, however, changes in mineral surface areas will cause the reaction path followed by the fluid to evolve continuously. In addition, even if equilibrium is assumed for all the minerals in the system except the irreversibly dissolving mineral, the eventual disappearance of this phase at certain points in space also results in the fluid experiencing more than one reaction path as it moves down a flow path (LICHTNER, 1988a,b). An example of this kind of phenomenon might be found in a weathering profile developed on a granite where the uppermost portion of the profile no longer contains any of the minerals originally found in the rock. Since one or more of the secondary minerals will be the irreversibly dissolving phase at the top of the profile, the reaction path followed in that portion of the flow path will be different from the one experienced by the fluid when it reaches the original feldspar-bearing rock at depth. Hence, in many cases it is necessary to consider physical space as well in describing the chemical evolution of a water. Where the reaction path changes with time, only *open system* models can describe water-rock interaction (LICHTNER, 1988b).

As a simple example of a reaction-flow system, consider the irreversible transformation of K-feldspar to kaolinite

driven by the influx of rain water. The overall reaction can be written in two parts: as a congruent dissolution reaction of K-feldspar plus a precipitation reaction in which the dissolved constituents combine to form kaolinite

$$2KAlSi_3O_8 + 8H^+ \xrightarrow{k1} 2K^+ + 2Al^{3+} + 6SiO_{2(aq)} + 4H_2O \quad (1)$$

$$2Al^{3+} + 2SiO_{2(aq)} + 5H_2O \xrightarrow{k2} Al_2Si_2O_5(OH)_4 + 6H^+. \quad (2)$$

Note that in this formulation, each reaction is characterized by its own rate constant, k_i. Since the fluid is not stationary, we need to include transport in addition to reaction in a quantitative formulation of the system. We can write a partial differential equation describing the conservation of mass of a species in solution, which in its most general form is given by

$$\frac{\partial(\phi c_i)}{\partial t} = -\sum_{\alpha} \nabla \cdot J_\alpha - R_i \quad (i = 1, 2, \ldots, N_c) \quad (3)$$

where c_i is the concentration of some species in solution, N_c is the number of independent chemical components which completely describe the system, ϕ is the porosity, $\nabla \cdot J_\alpha$ is the divergence of the various fluxes affecting the given species (e.g., advective, dispersive, and diffusive fluxes), and R_i (in units of moles per unit volume rock per unit time) is the sum of all the heterogenous (mineral-water) reactions that modify the concentration of species i in solution (LASAGA, 1984; LICHTNER, 1985; STEEFEL and LASAGA, 1990). We will therefore have one partial differential equation for each of the independent chemical components in the system.

As an example, if we assume that equilibrium exists between each of the various species of Al present in solution, then we can write the differential equation in terms of the total concentration of Al (REED, 1982; LICHTNER, 1985; KIRKNER and REEVES, 1988), which in the one-dimensional case is given by

$$\frac{\partial(\phi C_{Al_{tot}})}{\partial t} = -\frac{\partial}{\partial x}\left[-D\frac{\partial(\phi C_{Al_{tot}})}{\partial x} + \phi v C_{Al_{tot}}\right] - R_{Al} \quad (4)$$

where $C_{Al_{tot}}$ is the total concentration of Al in solution, D is the combined hydrodynamic dispersion and molecular diffusion coefficient (BEAR, 1979), v is the fluid velocity, and R_{Al} is the sum of the heterogeneous reactions which affect the concentration of Al. In the simple case in which we are considering only K-feldspar and kaolinite, the reaction term is given by

$$R_{Al} = R_{kspar} + 2R_{kaol} \quad (5)$$

where R_{kspar} and R_{kaol} are the reaction rates (in units of moles mineral per m^3 rock per unit time) of K-feldspar and kaolinite, respectively (taken as positive for precipitation and negative for dissolution) and the 2 in front of the precipitation rate of kaolinite reflects the number of Al ions in one formula unit of kaolinite. Note that the reaction rates for K-feldspar and kaolinite are not independent since they are coupled through the saturation state of the solution (see next section). By expressing the mineral-water reaction rates in terms of the saturation state, the independent chemical species in solution become the only unknowns in the conservation equations (Eqn. 3). When the Al conservation equation is solved simultaneously with similar expressions for the other independent species in solution (e.g., H^+, K^+, $SiO_{2(aq)}$, etc.), then we have a complete description of both the multi-component reactions and transport in the system. The numerical procedure for solving the full set of nonlinear partial differential equations in space and time is discussed in Appendix I.

KINETICS OF MINERAL-WATER REACTIONS

Rate Laws

In a general form, the rate of growth or dissolution of a mineral in aqueous solution can be written as

$$\text{Rate} = Akf(\Omega), \quad (6)$$

where A is the reactive surface area of the mineral of interest (m^2 per m^3 total rock), k is the rate constant (moles formula units mineral per m^2 per second), and $f(\Omega)$ is some function of the saturation state of the solution. The saturation state of the solution with respect to the reacting mineral is described by

$$\Omega = \frac{\text{IAP}}{K_{eq}}, \quad (7)$$

where IAP is the dissolved ion activity product written for the dissolution reaction and K_{eq} is the corresponding equilibrium constant. The rate law may contain additional terms describing the dependence of the rate on solution pH (GRANDSTAFF, 1977; CHRISTOFFERSEN, 1980; SCHOTT et al., 1981; AAGAARD and HELGESON, 1982; LASAGA, 1984; WOLLAST and CHOU, 1985; CARROLL-WEBB and WALTHER, 1988; KNAUSS and WOLERY, 1986, 1987, 1989; BLUM and LASAGA, 1988; BRADY and WALTHER, 1989; VAN CAPPELLEN and BERNER, 1990) and on the dissolved concentrations of surface-active solutes (NESTAAS and TERJESEN, 1969; OHARA and REID, 1973; BERNER et al., 1978; SJÖBERG, 1978; GRANDSTAFF, 1980; BOISTELLE, 1982; CHRISTOFFERSEN and CHRISTOFFERSEN, 1984; REDDY, 1986; SCHENK et al., 1989; DOVE and CRERAR, 1990; BURTON and WALTER, 1990; VAN CAPPELLEN and BERNER, 1990), but for the sake of simplicity, these dependencies are not explicitly included here.

Data on the dissolution kinetics of minerals in aqueous solution have been accumulating rapidly in recent years (e.g., WOLLAST, 1967; BERNER and MORSE, 1974; HOLDREN and BERNER, 1979; LIN and CLEMENCY, 1981; SCHOTT and BERNER, 1983, 1985; CHOU and WOLLAST, 1984; BALES and MORGAN, 1985; SCHOTT and PETIT, 1987; CASEY et al., 1988), and compilations of dissolution rate constants and activation energies are becoming available (SCHOTT and PETIT, 1987; WIELAND et al., 1988; MURPHY and HELGESON, 1989; MADÉ and FRITZ, 1989). With some exceptions, for example carbonates, data on growth rates of geologically important minerals are much less abundant (NANCOLLAS and REDDY, 1971; SAYLES and FYFE, 1973; BERNER et al., 1978; PLUMMER et al., 1979; RIMSTIDT and BARNES, 1980; INSKEEP and BLOOM, 1985; NIELSEN, 1986; ZAWACKI et al., 1986;

PHELAN and MATTIGOD, 1987; INSKEEP and SILVERFTOOTH, 1988; NAGY et al., 1988; RENDERS and BARNES, 1989; VAN CAPPELLEN and BERNER, 1990; NAGY et al., 1990).

In this paper, we use the following empirical form for the rate law of crystal growth and dissolution

$$\text{Rate} = Ak(\Omega^m - 1)^n \quad (8)$$

where k is either the growth or dissolution rate constant, and m and n are two adjustable positive numbers. By convention, the rate in Eqn. (8) is positive when the solution is supersaturated with respect to the mineral (precipitation) and negative when undersaturated (dissolution). Wherever possible, measured rate constants for growth and dissolution have been used in the simulations presented in this paper (Table 1).

Experimental growth rates for a large number of simple inorganic salts in aqueous solution follow the so-called parabolic law, which can be derived theoretically by assuming that the rate-determining step of the growth reaction is the integration of ions at growth sites along dislocation-induced surface steps (NIELSEN, 1982, 1984, 1986). In the parabolic rate law, the reaction order n is equal to 2 and m is the inverse of the number of ions per formula unit of the mineral. The normalized quantity Ω^m is also known as the saturation ratio. We have assumed this form for the growth rate of all minerals in the calculations.

The functional dependence on the saturation state of mineral dissolution reactions close to equilibrium is unknown in most cases. For K-feldspar, we have made the simple assumption that $m = n = 1$. In separate simulations, which are not shown here, we have tested a value of $m = 1/7$ (i.e., in this case, Ω^m is the normalized saturation ratio for K-feldspar). It was found that the effect on the overall behavior of the reaction system was relatively small, although the same is not true for changes in the formulation of the growth rate. The reason for this is that for different values of m, the dissolution rate always converges to the limiting value of AK with increasing undersaturation, while the growth rate diverges with increasing supersaturation.

Of the parameters which enter into the rate expression for a heterogeneous reaction, the reactive surface area is in general the least constrained. This is primarily because the surface areas of the reacting minerals are not constant with time. For a secondary mineral, surface area is initially created by nucleation and is subsequently modified by crystal growth and dissolution and by crystal ripening. Nucleation is an extremely important process to consider, since at supersaturation levels above a critical value, its rate may be very large (TURNBULL, 1950; POUND et al., 1954; NIELSEN, 1964; LOTHE and POUND, 1966; WALTON, 1967; DUNNING, 1969; FRANKL and VENABLES, 1970; TOSCHEV, 1973; BERNER, 1980; STUMM and MORGAN, 1981; ADAMSON, 1982), and therefore it may control the rate at which surface area is generated. In addition, the process of Ostwald ripening, whereby smaller crystals with higher solubility dissolve and reprecipitate as larger crystals (LIFSHITZ and SLYOZOV, 1961; WAGNER, 1961; CHAI, 1974, 1975; CRERAR et al., 1981; BARONNET, 1982; MARQUSEE and ROSS, 1983; MORSE and CASEY, 1988; EBERL et al., 1990) is important to include in the analysis as ripening counteracts rapid surface area generation by nucleation.

In our calculations we shall assume that the reactive surface area of a mineral is directly proportional to its total surface area. Although intuitively this assumption seems reasonable,

Table 1: Mineral-solution reactions at 25°C included in reaction-flow simulations, written in the direction in which they primarily go in the simulations. Where the backreaction occurs, the same formulation for the rate law and rate parameters are used. The parameters m and n are discussed in the text (Eqn. 8).

Mineral	Reaction	Log k (moles m^{-2} s^{-1})	Ref.	m	n	Log K_{eq}†
Kaolinite	$2Al^{+3} + 2SiO_{2(aq)} + 5H_2O \rightarrow Al_2Si_2O_5(OH)_4 + 6H^+$	-13.2	(1)	1/9	2	-7.43
K-feldspar	$KAlSi_3O_8 + 4H^+ \rightarrow K^+ + Al^{3+} + 3SiO_{2(aq)} + 2H_2O$	-11.5	(2)	1	1	0.08
Gibbsite	$Al^{+3} + 3H_2O \rightarrow Al(OH)_3 + 3H^+$	-11.8	(3)	1/4	2	-7.96
Quartz	$SiO_2 \rightarrow SiO_{2(aq)}$	-13.4	(4)	1	1	-4.00
Muscovite	$K^+ + 3Al^{+3} + 3SiO_{2(aq)} + 6H_2O \rightarrow KAl_2(AlSi_3O_{10})(OH)_2 + 10H^+$	-12.6	(5)	1/13	2	-14.56
Halloysite	$2Al^{+3} + 2SiO_{2(aq)} + 7H_2O \rightarrow Al_2Si_2O_5(OH)_4.2H_2O + 6H^+$	-12.2	(6)	1/9	2	-11.28

(1) Precipitation data at 80°C and pH 3 from NAGY et al. (1990), extrapolated to 25°C using an activation energy of 71 kJ/mole.
(2) HELGESON et al. (1984)
(3) Precipitation data at 80°C and pH 4 from STEEFEL et al. (in prep.), extrapolated to 25°C using an activation energy of 100 kJ/mole.
(4) RIMSTIDT and BARNES (1980)
(5) LIN and CLEMENCY (1981)
(6) Chosen to be 1 order of magnitude faster than kaolinite
† Thermodynamic data from EQ3NR data base (WOLERY, 1983), except for halloysite which is from HEM et al. (1973)

some laboratory and field studies suggest that it may be an oversimplification (NANCOLLAS and PURDIE, 1964; HOLDREN and SPEYER, 1985; ARENDS et al., 1987; WHITE and PETERSON, 1990) because the density of growth sites at the surface of a mineral may change over time.

Kinetics and Partial Equilibrium

What are the necessary conditions for attainment of partial equilibrium with respect to the secondary phases, and in those cases where it is not achieved, what is the behavior of the system? In the coupled K-feldspar dissolution-kaolinite precipitation reaction system represented by Eqns. (1) and (2), each reaction has its own rate constant, k_1 for the dissolution reaction and k_2 for the precipitation reaction. From Eqn. (8), it can be seen that the relative rates of the dissolution and precipitation reactions depend on the rate constants, the reactive surface areas of K-feldspar and kaolinite, and on the saturation state of the solution. If we define an effective rate coefficient, k', as the product of the reactive surface area of the mineral and its rate constant, we expect intuitively that where

$$\frac{k'_{\text{diss}}}{k'_{\text{ppt}}} = \frac{A_{\text{feldspar}} k_1}{A_{\text{kaolinite}} k_2} < 1 \qquad (9)$$

partial equilibrium with respect to kaolinite *could* be attained. Whether in fact this is true has been tested by solving Eqn. (3) numerically for the case in which a water undersaturated with respect to K-feldspar flows through the rock at a rate of 10 m^3 water per m^2 rock per year. Of the heterogeneous reactions listed in Table 1, only K-feldspar dissolution and kaolinite precipitation are considered in these simulations for the sake of clarity. Table 1 also gives the values of m and n used in the simulations. For the computation of the reaction rates, we use the 80°C precipitation data of NAGY et al. (1990) for kaolinite which has been extrapolated to 25°C using an activation energy of 71 kJ/mol. For K-feldspar, the reaction rate constant is taken from the data compiled and interpreted by HELGESON et al. (1984) based on a number of experimental studies. Table 2 lists the aqueous complexation reactions, assumed to be at equilibrium, which are included in the calculation. Table 3 gives aqueous concentrations and the saturation state of the solution with respect to the various mineral phases at the inlet.

In the simulations shown in Fig. 2, flow is from left to right, and the combined diffusion/dispersion coefficient is fixed at 5×10^{-3} m^2/a in this particular calculation. The reactive surface areas of K-feldspar and kaolinite are held constant for the approximately eight years required to achieve a steady state. The surface area of K-feldspar is taken as 1000 m^2 per m^3 rock, and the surface area of kaolinite is adjusted to give the appropriate ratio of the effective rate coefficients. Figure 2a shows that when the ratio of the effective rate coef-

Table 2: Complexation reactions considered in the simulations at 25°C.

Reaction	Log $K^{\dagger}_{eq}$
$H_2O = H^+ + OH^-$	-13.99
$Al(OH)^{++} + H^+ = Al^{3+} + H_2O$	4.93
$Al(OH)_2^+ + 2H^+ = Al^{3+} + 2H_2O$	10.07
$Al(OH)_3^\circ + 3H^+ = Al^{3+} + 3H_2O$	16.04
$Al(OH)_4^- + 4H^+ = Al^{3+} + 4H_2O$	22.20
$H_3SiO_4^- + H^+ = SiO_{2(aq)} + 2H_2O$	9.82
$CO_3^{--} + H^+ = HCO_3^-$	10.34
$CO_{2(aq)} + H_2O = H^+ + HCO_3^-$	-6.37

† Thermodynamic data from the EQ3NR data base (WOLERY, 1983).

Table 3: Inlet composition and saturation state of rainwater at 25°C, pH = 5.0, and pCO_2 = 1 bar (based on BERNER and BERNER, 1987).

Component	Log Total Concentration (M)	Mineral	Saturation (Log Ω)
K^+	-6.00	Kaolinite	-6.35
Al^{+++}	-8.00	K-feldspar	-12.46
$SiO_{2(aq)}$	-6.00	Gibbsite	-1.46
$Cl^{-(1)}$	-4.98	Quartz	-1.96
		Muscovite	-13.95
		Halloysite	-10.20

(1) Calculated from charge balance.

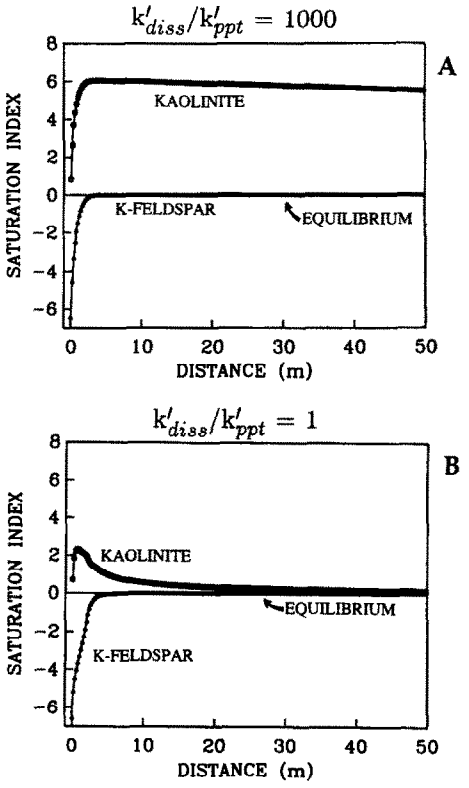

FIG. 2. Simulations with constant reactive surface areas of kaolinite and K-feldspar. Saturation indices (log Ω) of kaolinite and K-feldspar at steady state are plotted versus distance along the flow path. The Darcian flux is 10 m/a from left to right. The surface area of K-feldspar in each case is 1000 m^2 m^{-3} rock. The inlet fluid is an average continental rain water (Table 3). As the fluid moves along the flow path, the irreversible dissolution of K-feldspar quickly causes precipitation of kaolinite. (a) Where the ratio of the effective rate coefficients of K-feldspar dissolution to kaolinite precipitation is equal to 1000, equilibrium with respect to kaolinite is not achieved over the 25 m of the flow path. (b) With a ratio of the effective rate coefficients of K-feldspar and kaolinite = 1, the partial equilibrium approximation is justified.

ficients of the dissolution and precipitation reactions is equal to 1000, equilibrium with respect to kaolinite is not achieved over the 25 m of the flowpath. In this case, as suggested by Eqn. (9), the assumption of partial equilibrium would not be justified. In contrast, where the ratio of the effective rate coefficients is equal to 1, equilibrium with respect to kaolinite is achieved after a relatively short distance along the flowpath (Fig. 2b).

In Fig. 2a, the ratio of the effective rate coefficients for K-feldspar and kaolinite is equal to 1000. Hence, close to the inlet, the rate of K-feldspar dissolution is larger than the rate of kaolinite precipitation, causing the supersaturation of the solution with respect to kaolinite to rise until the rate of kaolinite precipitation becomes large enough to keep up with the dissolution of K-feldspar. Therefore, at a short distance from the inlet, the system achieves a steady state where the ratio of the actual rates of K-feldspar dissolution and kaolinite precipitation is on the order of the value of 2 expected if Al is conserved, despite the fact that the ratio of the effective rate constants is 1000 (Fig. 3). This fundamental tendency of the coupled dissolution-precipitation reaction system to evolve towards a steady state in which the rates of the reactions are nearly in balance is a result of the feedback of the saturation state of the solution on the rates of the heterogeneous reactions (Eqn. 8). It is important to note, however, that the near-conservation of Al does not require that the solution be at equilibrium with respect to the secondary phase. The distance from equilibrium with respect to the secondary phase at which a quasi-steady state is achieved increases with an increasing ratio of the effective rate coefficients, $k'_{\text{diss}}/k'_{\text{ppt}}$.

Although these simulations serve to illustrate the behavior of a reacting flow system as a function of the relative rates of the dissolution and precipitation reactions, they are inherently unrealistic because the surface areas of the reacting minerals are held constant. A complete treatment of water-rock interaction requires an explicit calculation of reactive surface areas along a flowpath. This is the subject of the remainder of the paper.

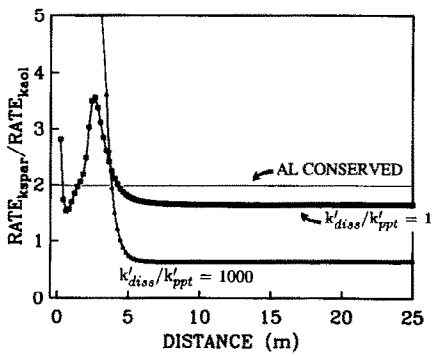

FIG. 3. Simulations with constant reactive surface areas of kaolinite and K-feldspar. The ratios of the rate of dissolution of K-feldspar over the rate of precipitation of kaolinite are plotted versus distance along the flow path at steady state. For the case where $k'_{\text{kspar}}/k'_{\text{kaol}}$ = 1000, the ratio of the rates comes relatively close to the value of 2 expected if Al is conserved despite the fact that the solution is not at equilibrium with respect to kaolinite. Hence, a short distance away from the inlet, the rate of kaolinite precipitation has increased so as to nearly balance the rate at which K-feldspar is dissolving.

EVOLUTION OF REACTIVE SURFACE AREA: THEORY

Nucleation

For nucleation of a mineral to occur, a free energy barrier must be overcome. The origin of this barrier to nucleation is the positive contribution of the interfacial free energy to the total free energy change associated with the precipitation of a crystal from solution (GIBBS, 1928; MCDONALD, 1962; NIELSEN, 1964; WALTON, 1967; BERNER, 1980). The height of the barrier, ΔG^*, can be regarded as the activation energy barrier to the nucleation process (NIELSEN, 1964; WALTON, 1967; DUNNING, 1969; TOSCHEV, 1973). A small solid cluster whose free energy of formation equals the maximum value, ΔG^*, is known as a critical nucleus. For homogeneous nucleation of spherical nuclei from solution, we have (for example, WALTON, 1967)

$$\Delta G^* = \frac{16\pi\sigma^3 v^2}{3(k_b T \ln \Omega)^2} \tag{10}$$

where v is the volume of a formula unit of the mineral and σ is the solid-solution interfacial free energy. Equation (10) shows that the activation energy of the nucleation process decreases with increasing solution saturation and with increasing temperature. According to the classical theory of nucleation, the steady-state rate of homogeneous nucleation can be written (VOLMER, 1945; WALTON, 1967; DUNNING, 1969; TOSCHEV, 1973)

$$\frac{dN}{dt} = J = J_o \exp\left(\frac{-\Delta G^*}{k_b T}\right) \tag{11}$$

where N is the number of nuclei per unit volume overcoming the activation barrier and J_o is a pre-exponential factor whose value for homogeneous nucleation in solution at 25°C is in the range from 10^{20} to 10^{37} m^{-3} sec^{-1} (NIELSEN, 1964; WALTON, 1967; VAN CAPPELLEN, 1990).

In the case of heterogeneous nucleation the interfacial free energy arises from the creation of interface between the nucleus and both the aqueous solution and the substrate upon which it is formed (see Appendix II)

$$\Delta G_{\text{interface}} = A_{cw}\sigma_{cw} + A_{cs}(\sigma_{cs} - \sigma_{sw}) \tag{12}$$

where A_{cw} is the surface area between nucleus and solution, A_{cs} is the surface area between nucleus and substrate, σ_{cw} is the crystal-solution interfacial energy, σ_{cs} is the crystal-substrate interfacial energy, and σ_{sw} is the substrate-solution interfacial energy. In certain cases it may be possible to estimate the value of σ_{cs} from the degree of lattice mismatch between the precipitate and the mineral substrate (e.g., VAN DER MERWE and BALL, 1975). In the treatment which follows, however, we make the simplifying assumption that the interfacial free energy of the nucleus is due entirely to the excess solid-solution interfacial area created in forming the nucleus ($=A_{cw} - A_{cs}$). The crystal-substrate and substrate-solution interfacial tensions can then be eliminated from Eqn. (12). If, in addition, we take the geometry of the nucleus as a half-sphere on a planar substrate, we have

$$\Delta G_{\text{interface}} = \pi r^2 \sigma_{cw} \tag{13}$$

where r is the radius of the nucleus. The free energy of formation of the critical nucleus then becomes (see Appendix II)

$$\Delta G^* = \frac{\pi\sigma^3 v^2}{3(k_b T \ln \Omega)^2}. \quad (14)$$

It is clear that Eqn. (14) only offers a crude calculation of the activation energy barrier for heterogeneous nucleation. Nevertheless, the formulation for nucleation presented here reproduces at least qualitatively the well-known observation that heterogeneous nucleation is characterized by a significantly lower activation energy barrier than homogeneous nucleation. The formulation used to calculate the pre-exponential factor for heterogeneous nucleation is discussed in Appendix II.

In both homogeneous and heterogeneous nucleation, the nucleation rate depends exponentially on the activation energy, ΔG^*. If, for the mineral of interest, the nucleation rate is plotted versus the saturation, a typical curve is obtained (Fig. 4). The curve is characterized by a critical supersaturation below which the nucleation rate is extremely small and above which the nucleation rate increases very rapidly. Let us think of what this means in terms of the generation of reactive surface area. At supersaturations above the critical value, new surface area is created mainly by the nucleation of additional crystallites. We shall refer to this regime of surface area generation as *nucleation-controlled.* At supersaturations below the critical value, surface area generation is *crystal growth-controlled,* i.e., surface area increases by growth of existing crystals.

The rate of surface area generation is large in the nucleation-controlled domain because of the large surface to mass ratio of small crystallites. Hence, if a solution composition were to start in the nucleation-controlled regime above the critical supersaturation value, the generation of surface area of the secondary mineral by nucleation would rapidly increase the effective rate coefficient, $k' = Ak$, causing the solution supersaturation to collapse to at least the critical value. Therefore, in geological environments, a degree of supersaturation above the critical value is forbidden other than for very short periods of time.

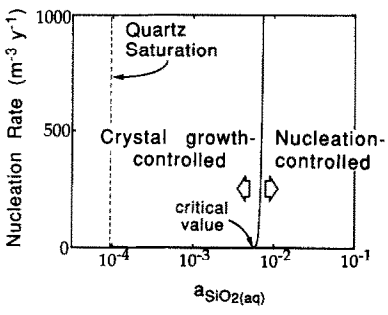

FIG. 4. Rate of heterogeneous nucleation of quartz at 25°C plotted versus the activity of $SiO_{2,aq}$ (solid line). The calculation assumes an interfacial energy of 350 mJ/m^2 and a substrate surface area of 1000 m^2 mineral per m^3 rock, and is based on the formulation given in Appendix II. Surface area generation will be nucleation-controlled, and therefore very rapid, at $SiO_{2,aq}$ activities above the critical value and crystal growth-controlled at activities below this value.

Table 4: Some mineral-aqueous solution interfacial free energies.

Substance	σ (mJ m^{-2})	Reference
Amorphous Silica	46	ALEXANDER et al. (1954)
Quartz	335-385	PARKS (1984)
Apatite Precursor	26	VAN CAPPELLEN (1990)
Fluorapatite	289	VAN CAPPELLEN (1990)
Gibbsite (001)	140	SMITH and HEM (1972)
Gibbsite (100)	483	SMITH and HEM (1972)
$Cu(OH)_2$	410	SCHINDLER (1967)
Calcite	97	VAN CAPPELLEN (1990)
Cerussite	125	NIELSEN and SÖHNEL (1971)
Barite	135	NIELSEN and SÖHNEL (1971)
ZnO	770	SCHINDLER (1967)
CuO	690	SCHINDLER (1967)
Hematite	1200	BERNER (1980)
Goethite	1600	BERNER (1980)
Kaolinite	>200	This study

Mineral-Solution Interfacial Energies

A critical parameter determining the rate of nucleation of a mineral is its interfacial free energy with respect to solution (see Eqn. 14). Interfacial energies (or surface tensions) for a number of geologically important minerals in water are given in Table 4. We find a large range in interfacial energies from as low as 26 mJ/m^2 for a poorly crystalline calcium phosphate to as high as 1600 mJ/m^2 for goethite. Minerals like quartz and gibbsite, which have relatively large interfacial free energies, will nucleate slowly at low temperatures, even in the presence of favorable substrates. In contrast, materials like amorphous silica and poorly crystalline calcium phosphate are characterized by low interfacial energies and thus will nucleate easily once the solution composition exceeds their solubility. As a generalization, substances with low interfacial energies tend to be less well crystalline and have higher solubilities than their more stable analogues (NIELSEN and SÖHNEL, 1971; VAN CAPPELLEN, 1990). As an example, compare the solubilities and interfacial energies of quartz and amorphous silica.

Precursors

A stable secondary mineral which would otherwise be difficult or impossible to nucleate at low temperatures because of its high critical supersaturation for heterogeneous nucleation may circumvent this problem by making use of a more soluble precursor with a lower interfacial energy. A precursor phase is usually amorphous or poorly crystalline, and it may have a chemical composition distinct from that of the final stable mineral (e.g. BERNER, 1970, 1984; LANGMUIR, 1971; LANGMUIR and WHITTEMORE, 1971; VAN CAPPELLEN, 1990). It rapidly nucleates when the solution exceeds its solubility, driving the solution composition toward saturation with the precursor. Although the reaction pathways are poorly known, it appears that precursors are replaced by more stable minerals through solution mediated processes (MORSE and CASEY, 1988; CHRISTOFFERSEN et al., 1989).

In the case of calcium phosphate precipitation from artificial seawater, it is observed that after the initial nucleation of a precursor, stable fluorapatite starts forming when the solution is still supersaturated with respect to the precursor

(VAN CAPPELLEN, 1990). Apparently, fluorapatite is able to use some fraction of the precursor surface as a template for its own growth, in effect circumventing the need for direct nucleation. This *cannibalistic* use of a precursor surface by a more stable mineral forms the basis for the mathematical formalism we have developed to describe mineral formation via a precursor (Appendix III). Once it grows, the stable phase can increase its own surface area until it can control the composition of the solution. When this happens, the saturation state of the solution moves below the solubility of the precursor, causing the latter to dissolve.

The initial precipitation of a precursor has the effect of extending the nucleation-controlled domain of surface area generation to saturations close to the solubility of the precursor. As a concrete example, consider the case of quartz and amorphous silica at 25°C using the interfacial energies listed in Table 4. If the nucleation rates of quartz and amorphous silica (in units of nuclei per m^3 rock per year) are plotted versus dissolved silica activity, it is evident that amorphous silica rather than quartz will nucleate directly because of its lower critical dissolved silica concentration for nucleation (Fig. 5). To a first approximation it is possible to calculate the rate of surface area generation by multiplying the nucleation rate by the surface area of the critical nucleus of amorphous silica. If the nuclei are half-spheres and the total surface area of available substrate equals 1000 m^2 in a m^3 of rock, then the rate of surface area generation for a dissolved silica activity only 5% higher than saturation with amorphous silica equals 6000 $m^2\ m^{-3}\ a^{-1}$! This rapid generation of amorphous silica surface area will ensure that the activity of $SiO_{2(aq)}$ cannot remain for long above saturation with respect to amorphous silica. It is amorphous silica's ability to nucleate easily, and not any intrinsic feature of its growth rate (recent data indicates the growth rate constant for amorphous silica is only slightly higher than that of quartz; RENDERS and BARNES, 1989), that explains why amorphous silica saturation is an upper limit for $SiO_{2(aq)}$ activities in natural aqueous systems (SIEVER, 1957).

In many instances the replacement of a precursor by a more stable phase occurs so rapidly that it may be difficult to physically isolate the precursor. Typically in experiments

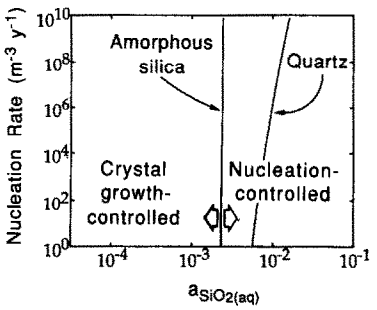

FIG. 5. Rates of heterogeneous nucleation of quartz and amorphous silica at 25°C using interfacial energies of 350 and 46 mJ/m^2 for quartz and amorphous silica, respectively. The figure shows that amorphous silica will nucleate rather than quartz because of its lower interfacial energy, thus extending the nucleation-controlled regime down to $SiO_{2,aq}$ activities close to the solubility of amorphous silica at 2×10^{-3} M.

where solution saturation is allowed to decrease progressively, the precursor is detected by plotting the concentration or saturation of the solution versus time (e.g., NIELSEN and TOFT, 1984) or by plotting the overall rate of precipitation versus time (VAN CAPPELLEN, 1990). The presence of the precursor is then identified as a distinct inflection in the curves, reflecting the dissolution of the precursor as the solution becomes undersaturated with respect to this phase. In other instances the precursor, or more often, an intermediate phase occurring between the initial precursor and the final, most stable mineral may be long-lived. Where this is the case, the presence of the precursor or intermediate phase provides definite constraints on the interfacial energy of the more stable mineral, since we know that if the latter nucleated easily, then the metastable phase should not have formed at all (see section on halloysite and kaolinite).

Ostwald Ripening

Small crystals have a higher solubility than large crystals because of their greater surface area per unit mass. This forms the driving force for Ostwald ripening, which involves a redistribution of mass from the smaller crystals in the system to the larger crystals. For a given degree of supersaturation with respect to the bulk mineral, the solution is saturated with particles of size r^*, given by (e.g., NIELSEN, 1964)

$$r^* = \frac{2\sigma V_o}{RT \ln (C/C_{eq})} \tag{15}$$

where C is the concentration of the mineral in solution, C_{eq} is the bulk solubility (i.e., the solubility of very large particles), and V_o is the molar volume of the mineral. Equation (15) is known as the Gibbs-Kelvin equation. For mineral grains with $r < r^*$, the solution is undersaturated, and these particles will tend to dissolve and reprecipitate as larger crystals. Because Ostwald ripening involves a mass transfer from smaller crystals to a lesser number of large crystals, it has the effect of decreasing the total number of crystals in the system. The ratio of the solubility of a grain of radius r and the bulk concentration C can be obtained from the Gibbs-Kelvin equation (NIELSEN, 1964):

$$\frac{C_r}{C} = \exp\left[\frac{2\sigma V_o}{RT}\left(\frac{1}{r} - \frac{1}{r^*}\right)\right]. \tag{16}$$

Equation (16) indicates that the origin of the driving force for Ostwald ripening lies in the interfacial free energy of the mineral, σ.

Crystal Size Distributions

Any attempt at a quantitative estimation of the time required to achieve equilibrium with a secondary mineral must treat the generation of reactive surface area through the nucleation of the mineral or its precursor and the subsequent increase in mineral surface area due to crystal growth. In addition, it is important to consider the effects of crystal ripening because of its role in modifying the large amounts of surface area created by nucleation. Obviously, then, in a realistic simulation of reactive surface evolution, the number of crystals of a given size will vary with time. The most

straightforward way to deal with this problem is to define a continuous variable for the crystal size distribution (NIELSEN, 1964; MARQUSEE and ROSS, 1983; RANDOLPH and LARSON, 1988). Following RANDOLPH and LARSON (1988) we define the population density, n, by

$$n = \frac{dN}{dr} \tag{17}$$

where N is the cumulative number of crystals up to a radius r. The number of crystals between any two grain sizes r_1 and r_2 is obtained by integrating n between these two limits (RANDOLPH and LARSON, 1988):

$$\int_{r_1}^{r^2} n dr = \Delta N. \tag{18}$$

A "population balance" or continuity equation for the population density can be written to describe the time evolution of the crystal size distribution for a closed system (i.e., one in which there is no physical transport of crystals into or out of the system). In the continuity equation, crystal growth and dissolution will appear mathematically as advection terms as crystals grow into and out of a specific size:

$$\frac{\partial n}{\partial t} = -v_c \frac{\partial n}{\partial r} \tag{19}$$

where v_c is the linear growth or dissolution rate of the mineral (in units of length per unit time), taken outside of the derivative because it is independent of grain size. In the case of precipitation, nucleation becomes the boundary condition at the minimum grain size n_o, which is the critical radius of nucleation.

Perhaps the simplest way to derive an expression for Ostwald ripening in terms of the population density is to consider the problem as one in which mass or mineral volume (since the density of the mineral is constant) is conserved. In this way, we decouple mathematically the changes in population density due to ripening from those of growth and dissolution. The continuity equation for volume conservation during ripening is, then,

$$\frac{\partial V}{\partial t} = -\frac{\partial}{\partial r}[v_{ost}(r)V] \tag{20}$$

where V is the volume of crystals of a given size per unit volume rock (volume density) and v_{ost} is the Ostwald ripening rate which remains inside the derivative because it is a function of the grain size r. The term v_{ost} represents a pseudo-growth rate which can be thought of as the rate at which smaller particles combine to form crystals of larger size. The ripening rate is applied to the distribution (rather than to individual crystals) and is therefore always positive. In this respect, it is similar to some of the formulations used to describe the process of agglomeration (RANDOLPH and LARSON, 1988, p. 294). The rate of coarsening is proportional to the degree of undersaturation of a particular grain size with respect to the concentration of the bulk solution, so that for $r < r^*$, we have

$$v_{ost}(r) = V_o k\left[\frac{C_r}{C} - 1\right] \tag{21}$$

where the driving force for the ripening, C_r/C is obtained from Eqn. (16). Equations (16) and (21) indicate that the smallest crystals in the distribution will ripen the most rapidly because they are far from equilibrium.

If we assume a spherical geometry, the relationship between volume density and population density becomes

$$V = n\tfrac{4}{3}\pi r^3. \tag{22}$$

Substituting Eqn. (22) into Eqn. (20), an expression for Ostwald ripening in terms of the population density can be written

$$\frac{\partial n}{\partial t} = -\frac{\partial}{\partial r}[v_{ost}(r)n] - \frac{3v_{ost}(r)n}{r}. \tag{23}$$

Note that the continuity equation in the case of Ostwald ripening has a decay term which reflects the fact that as small crystals recombine to form a lesser number of larger crystals, the total number of crystals in the system must decrease.

As an illustration, consider the ripening of an initial Gaussian distribution of gibbsite crystals with an average radius of 0.1 μm. In calculating the ripening rate, we use a mean gibbsite interfacial energy of 350 mJ/m^2 (as an approximate average of the edge and 001 interfacial energies determined by SMITH and HEM, 1972). The governing continuity equation is solved using a standard finite difference discretization based on upstream weighting to ensure stability (PRESS et al., 1986). Figure 6 shows that the population increases in grain size and that the total number of crystals in the system decreases, reflected by smaller areas under the curves with increasing time.

Population Balance

The linear growth/dissolution rate and the Ostwald ripening rate can be combined in a single equation to calculate the crystal size distribution of a mineral as a function of time:

$$\frac{\partial n}{\partial t} = -v_c \frac{\partial n}{\partial r} - \frac{\partial(v_{ost}(r)n)}{\partial r} - \frac{3v_{ost}(r)n}{r}. \tag{24}$$

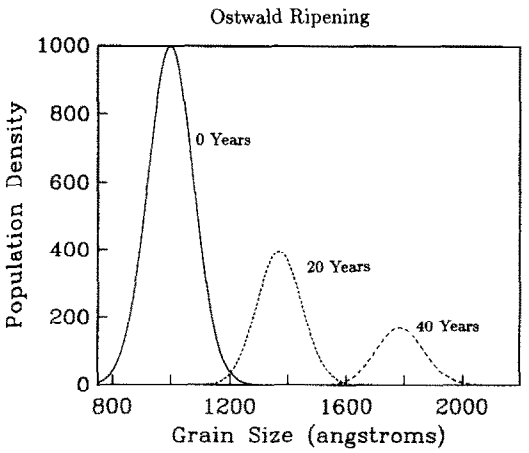

FIG. 6. Ostwald ripening of an initially Gaussian population of gibbsite crystals with an average size of 1000 Å using an interfacial free energy of 350 mJ/m^2. The distribution moves to larger grain sizes, and the total number of crystals in the system decreases with time.

This equation is integrated numerically between the limits of the critical nucleus size and an upper limit greater than the size obtained by any of the crystals in the system. The nucleation rate determines the addition of crystals of critical size to the crystal population.

By combining a computation of the crystal size distribution with the reaction-flow simulations described in the section on reaction-flow, we have the means to calculate the evolution of reactive surface area as a function of both time and space. The equations must be solved numerically because neither the nucleation rate nor the crystal growth/dissolution rate will be constant with time.

APPLICATION

Halloysite and Kaolinite

Halloysite is one of the most important geological examples of a metastable phase forming prior to the appearance of the more stable secondary mineral, in this case kaolinite (PARHAM, 1969a,b; KITTRICK, 1969; ANAND et al., 1985; KRONBERG et al. 1987; RAYMAHASHAY et al., 1987). Halloysite is defined by CHURCHMAN and CARR (1975) as a mineral having a kaolinite structure containing interlayer water. There is considerable evidence to suggest that halloysite itself often forms from an amorphous aluminosilicate precursor, usually having an Al to Si ratio corresponding to that of allophane (PARHAM, 1969a,b; SIEFFERMANN and MILLOT, 1969; TSUZUKI and KAWABE, 1983; SALTER and MURRAY, 1989). Hence, halloysite is in most cases an intermediate phase rather than a true precursor.

PARHAM (1969a,b) was one of the first workers to recognize the widespread occurrence of halloysite in weathering profiles. In Cretaceous weathering profiles from Minnesota, PARHAM (1969a) proposed that the paragenetic sequence consisted of allophane → halloysite → pseudo-hexagonal kaolinite. He also noted that kaolinite was the dominant mineral toward the top of the profile while halloysite was abundant at depth, i.e., closer to the zone of weathering of fresh parent rock. As a modern analogue, PARHAM (1969a) studied deep weathering profiles in granite in Hong Kong and found that kaolinite was minor to absent. Where kaolinite was found, it appeared to be forming from halloysite rather than directly from weathering of feldspar. SIEFFERMANN and MILLOT (1969) studied a number of weathering profiles developed on basalt in Cameroon and characterized by differing annual rainfalls. In areas having annual rainfalls of about 10 m/a and no dry season, they observed that allophane was converted to well-crystalline kaolinite and gibbsite. In contrast, where the annual rainfall was between 3 and 6 m/a with an approximately three-month dry season, they found the sequence allophane → halloysite. They also observed that allophane was more abundant at depth while halloysite predominated close to the top of the profile. This spatial zoning in which the thermodynamically least stable phase is found toward the base of the profile has been noted in a number of studies of the weathering environment (PARHAM, 1969a; SIEFFERMANN and MILLOT, 1969; SALTER and MURRAY, 1989; INIGUEZ-RODRIGUEZ, 1981).

The frequent persistence of halloysite and allophane in weathering profiles constrains the interfacial free energy of kaolinite at low temperatures. In Fig. 7a the heterogeneous nucleation rate of kaolinite is calculated for a variety of interfacial tensions and then plotted versus the saturation index (log Ω) with respect to kaolinite. From the figure it appears likely that the interfacial tension for kaolinite is higher than 200 mJ/m^2. If the interfacial energy of kaolinite were below 200 mJ/m^2, then the rate of direct nucleation of kaolinite (and thus its rate of surface area generation) would be so large that significant amounts of halloysite would not form. Thus, the observed occurrence of halloysite provides an indirect way of estimating a minimum interfacial free energy for kaolinite in water. Because of the uncertainties in the mathematical formulation for heterogeneous nucleation, it is not possible to view Fig. 7a other than as a semi-quantitative result. However, it can be stated unequivocally that the common occurrence of halloysite and allophane confirm that direct nucleation of kaolinite is not the major mechanism by which kaolinite surface area is created at low temperatures.

The common occurrence of halloysite also provides some extremely important constraints on what the saturation state of the fluids with respect to kaolinite must have been as they moved through the weathering profiles. Clearly, these waters must have been significantly supersaturated with respect to kaolinite for at least part of their life history. This is corroborated by chemical analyses of low temperature natural waters (HEM et al., 1973; PAČES, 1978). Figure 7b shows a histogram of kaolinite saturation indices (log Ω) calculated from analyses of ephemeral and perennial springs from the Sierra Nevadas in FETH et al. (1964). The saturation calculations are corrected for the measured temperatures of the waters and are based on the thermodynamic data base in the EQ3NR code (WOLERY, 1983). Only those analyses for which dissolved

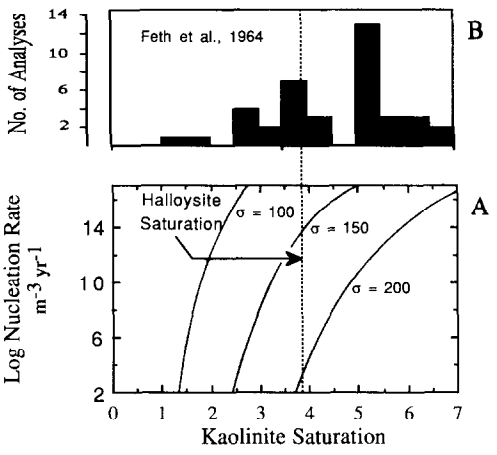

FIG. 7. (a) Heterogeneous nucleation rate of kaolinite versus its saturation index (log Ω) using interfacial energies for kaolinite of 100, 150, and 200 mJ/m^2. For interfacial energies of 100 and 150 mJ/m^2, the calculation predicts that the direct nucleation rate of kaolinite (and therefore the rate of surface area generation) will be so large that supersaturations should rapidly drop below halloysite saturation. The common occurrence of halloysite in weathering profiles, therefore, suggests that the interfacial energy of kaolinite must be greater than 200 mJ/m^2. (b) Water analyses from Sierra Nevada ephemeral and perennial springs (FETH et al., 1964) plotted versus kaolinite saturation index. Many of the waters are supersaturated with respect to kaolinite. Note the clustering of values around halloysite saturation.

Al is reported are included in Fig. 7b. The low amounts of dissolved Al in the other analyses imply that they would probably fall closer to saturation with respect to kaolinite. It is clear, however, that many of the spring waters are significantly supersaturated with respect to kaolinite. Figure 7a further shows a distinct clustering of values close to saturation with respect to halloysite. FETH et al. (1964) also observed that a number of the springs were actively precipitating amorphous aluminosilicate materials. These metastable phases provide additional evidence that the waters are not in all cases in equilibrium with respect to kaolinite.

It should also be apparent, however, that invoking metastable equilibrium with respect to halloysite or an amorphous aluminosilicate (e.g., HEM et al., 1973; PAČES, 1978) is an oversimplification of the problem as well, since both the chemical analyses of natural waters and the mineralogical observations suggest that the reaction systems are evolving gradually towards equilibrium with kaolinite. In contrast to the interpretation of natural water analyses reflecting metastable equilibrium with respect to various phases, the model proposed here for low temperature water-rock interaction is a completely kinetic one in which poorly crystalline or amorphous materials nucleate preferentially and are gradually replaced by minerals with higher crystallinities and lower solubilities.

Weathering

As an application of the concepts outlined above, we consider the weathering by rainwater of an initially fresh granite under tropical conditions. Such a situation might arise, for instance, where a slope failure suddenly exposes a mass of unaltered granite to weathering. By combining the numerical code for reactive flow outlined above and in Appendix I with a calculation of crystal size distributions for the secondary minerals in the system (Eqn. 24), it is possible to track the evolution of both the rock mineralogy and water compositions as the weathering profile develops. Since the simulations are carried out in one dimension, they cannot account for the nonlinear feedbacks between the mineral-solution reactions and the fluid flow which arise through porosity-permeability changes of the medium (see, e.g., ORTOLEVA et al., 1987; STEEFEL and LASAGA, 1990). Furthermore, because of the uncertainties in many of the parameters used here, it is not possible to rigorously estimate the time scale necessary to attain partial equilibrium (although observations of weathering profiles tell us that it must be relatively slow in the case of kaolinite). By including a reasonably realistic calculation of surface area evolution, however, the simulations give us a semi-quantitative picture of how a reaction front evolves in a reactive flow system.

The mineral-water reactions included in the simulations are given in Table 1 along with their rate and equilibrium constants. The numerical simulations are carried out at 25°C with the inlet concentrations and saturation states, corresponding to the average rainwater composition used in Fig. 2 (see Table 3). The timestep in the simulations starts at about 1 sec and gradually increases to a maximum of 10 years. A constant grid spacing of 0.1 m is used in all the simulations. An annual rainfall of 10 m/a, a number typical of a tropical climate without a dry season (SIEFFERMANN and MILLOT, 1969), is assumed. If the rainfall and flow through the weathering profile are constant, this results in a Darcian flux of 10 m^3 water per m^2 rock per year, which, for a constant porosity of 10%, yields a true velocity of 100 m per year. Initially, quartz and K-feldspar are the only minerals present in the rock, both of which begin with surface areas of 1000 m^2 per m^3 rock. As potential nucleators, we include the minerals gibbsite, halloysite, kaolinite, and muscovite. Halloysite is used here in a broad sense as a precursor for kaolinite. It is assigned a relatively small interfacial energy of 50 mJ/m^2 so that it nucleates easily, while a variety of interfacial energies for kaolinite are used to test the sensitivity of the simulations to this parameter. Gibbsite is assigned an interfacial energy of 225 mJ/m^2 and the interfacial free energy of muscovite is taken to be the same in each case as that of kaolinite. Note that the choice of an interfacial energy will determine both the nucleation rate and the rate of Ostwald ripening for that mineral.

In order to calculate the crystal size distribution for each of the secondary minerals, it is necessary to determine the initial size of the critical nucleus, which depends on both the interfacial free energy of the mineral and the supersaturation state of the solution (Appendix II). For the conditions considered here, the critical nuclei of the minerals range from 10 to 20 Å. In order to keep the bookkeeping involved in computing the crystal size as simple as possible, we use an initial radius of 10 Å for all of the secondary minerals. The crystal size distribution is computed by keeping track of 100 grain sizes at each point in space within the flow field.

The reactive flow simulations use a number of values for the interfacial free energy of kaolinite to illustrate the very strong effect this parameter has on the evolution of the system. This can be clearly seen by monitoring the saturation state of the fluid with respect to kaolinite at a fixed point in space 3 m from the inlet (Fig. 8a). We observe different kinds of behavior depending on whether kaolinite nucleates directly or whether it forms via a precursor. For example, if an interfacial free energy of 100 mJ/m^2 is chosen for kaolinite, Fig. 8a and b indicate that rapid generation of reactive surface area by direct nucleation of kaolinite brings the solution composition down below the solubility of halloysite within several years. Using an interfacial energy of 150 mJ/m^2, kaolinite still forms via direct nucleation, but the transition from nucleation-controlled to crystal growth–controlled surface area generation (marked by the abrupt decrease in the rate at which the solution supersaturation declines) occurs at a higher supersaturation than it does if 100 mJ/m^2 is used. If an interfacial energy of 225 mJ/m^2 is used for kaolinite, as suggested by the calculations presented in Fig. 7, the direct nucleation of kaolinite is too slow, and halloysite becomes the dominant phase formed in the early stages of rock alteration (Fig. 9). However, since a portion of the surface area of the halloysite is used by kaolinite, kaolinite is able to gradually increase its modal percentage so that by 7000 years, its volume fraction exceeds that of halloysite. During the period in which halloysite surface area is being appropriated by kaolinite, the solution remains close to halloysite saturation (Fig. 8a). Hence, although kaolinite is actively precipitating, the solution is in apparent equilibrium with the precursor.

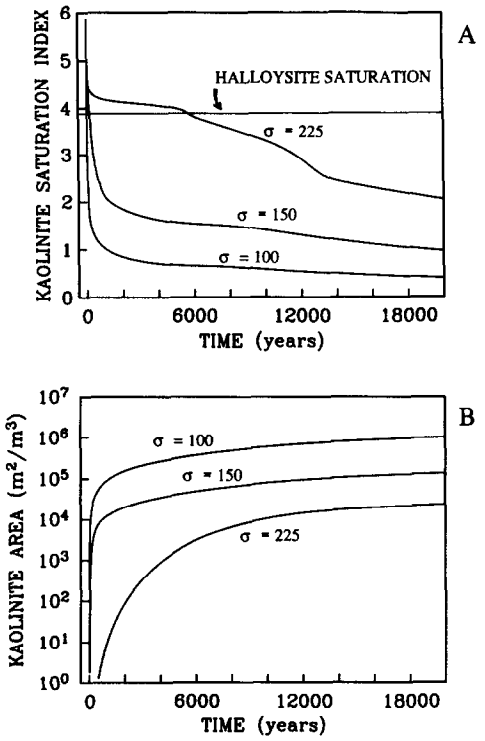

FIG. 8. Time evolution of kaolinite surface area and saturation index using various interfacial energies for kaolinite at a point 3 m from the inlet to the system. The mineral-solution reactions considered are given in Table 1 and inlet conditions are given in Table 3. (a) Saturation index for kaolinite versus time. Because of the rapid generation of surface area where the kaolinite interfacial free energy is 100 or 150 mJ/m^2, the supersaturation state of the solution quickly drops below halloysite saturation. For an interfacial free energy of 225 mJ/m^2, however, kaolinite forms via a halloysite precursor, so that the solution remains close to saturation with halloysite for approximately the first 6000 years. Eventually the reactive surface area of kaolinite increases sufficiently to bring the solution composition below halloysite saturation and the precursor completely dissolves. (b) Surface area of kaolinite calculated using interfacial free energies of 100, 150, and 225 mJ/m^2. Surface area generation is more rapid for smaller values of the interfacial free energy because of direct nucleation of kaolinite.

This explains the clustering of water analyses close to halloysite saturation shown in Fig. 7b. With further increase in the surface area of kaolinite, the supersaturation state of the solution finally drops to values below saturation with respect to halloysite, so that between 6000 and 14,000 years, halloysite dissolves (Fig. 9). Beyond 14,000 years, the rate of decrease of the supersaturation state of the solution reflects only the contribution due to crystal growth and ripening of kaolinite.

In those simulations where kaolinite forms via its precursor halloysite, the rate at which halloysite is converted to kaolinite is determined by the parameter P (Appendix III), the fraction of the halloysite surface area which can be used for growth by kaolinite. In the simulations described above, we used a value for P of 10^{-9} which results in the volume fraction of kaolinite exceeding that of halloysite at 7000 years. In contrast, if values of 10^{-8} and 10^{-10} are used, the kaolinite forms a larger percentage of the weathering profile than does halloysite by about 3500 and 14,000 years, respectively.

In the simulations, gibbsite did not nucleate in significant amounts because of its large interfacial energy and its large activation free energy for precipitation (Appendix II). In low temperature environments, formation of gibbsite probably occurs preferentially via a less crystalline precursor (SMITH and HEM, 1972; HEM and ROBERSON, 1990), so that more realistic simulations should include a gibbsite precursor as a potential nucleator. Muscovite did not nucleate in significant quantities in any of the simulations. The nucleation rate of muscovite is suppressed because kaolinite forms first along the reaction-flow path and therefore has the effect of reducing the saturation state of the solution to below the critical value for muscovite. The more rapid precipitation of kaolinite may explain why muscovite, or its equivalent illite, is not a major component of many weathering profiles even though, thermodynamically, it should be a stable phase.

Figures 10 through 12 illustrate the development of the weathering profile as a function of distance along the flow path through the rock, in this case using a value of 225 mJ/m^2 for the interfacial free energy of kaolinite and a value of 10^{-9} for P. Initially, nucleation rates of halloysite are large over appreciable distances from the flow inlet because the reactive surface areas are too low for the precipitation of secondary minerals to bring down the solution supersaturation (Fig. 10a and b). As the surface areas of the secondary minerals increase due to nucleation and crystal growth, however, the saturation state of the fluids decreases to a value close to metastable equilibrium with respect to halloysite (1000 a, Fig. 10c), resulting in a drop of the halloysite nucleation rate downstream of the developing reaction front (Fig. 10a). With the continued growth of kaolinite, the solution composition moves below halloysite saturation, so that by 10,000 years halloysite is dissolving over the entire 10 m of the flow path (Fig. 10c).

The growth of the secondary minerals halloysite and kaolinite at the expense of K-feldspar is most clearly illustrated by a plot of mineral volume percentages versus distance in the weathering profile (Fig. 11). At 10,000 years, halloysite makes up nearly 5% of the rock at the reaction front, its

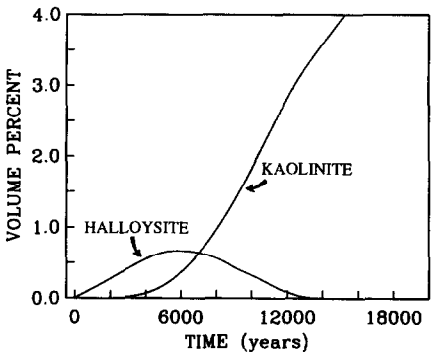

FIG. 9. Volume fractions of kaolinite and halloysite versus time 3 m from the inlet using an interfacial energy for kaolinite of 225 mJ/m^2. Because direct nucleation of kaolinite is slow in this case, halloysite is initially the dominant mineral. However, continued growth of kaolinite on the halloysite surface area eventually causes the solution to become undersaturated with respect to halloysite by about 6000 years.

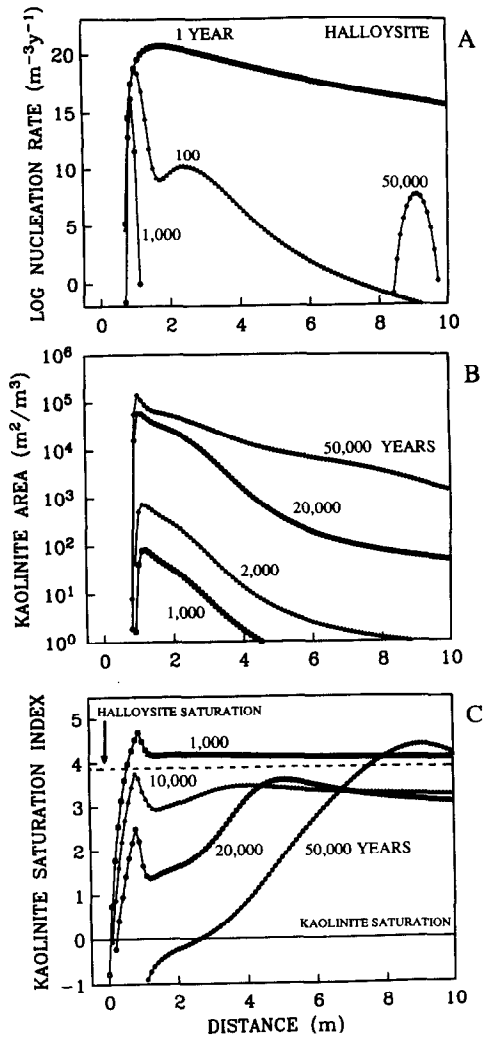

FIG. 10. Weathering of fresh granite. (a) Nucleation rate of halloysite which begins as broad curve at 1 year and gradually evolves to a sharper profile as the downstream solution saturation drops below the critical nucleation value for halloysite due to the precipitation of secondary minerals. See text for explanation of the incipient nucleation event at 50,000 years. (b) The surface area of kaolinite evolves with time as crystal growth continues. (c) Saturation index of kaolinite versus distance which changes due to the evolution of the kaolinite surface area. The increase in the degree of supersaturation downstream with time is the result of the fact that the K-feldspar dissolution front migrates into portions of the flow field which contain less kaolinite surface area. See text for further explanation.

profile having sharpened slightly from its distribution at 1000 years due to the effect of dissolution downstream of the front. By 20,000 years, the halloysite has disappeared completely because of the continued increase in the volume fraction of kaolinite. The volume percentage of K-feldspar with time presents the most straightforward pattern, gradually decreasing close to the top of the weathering profile until, by 50,000 years, it has dissolved completely from the first 4 m of the flow path. While the overall shape of the mineral volume fraction profiles may be relatively simple to interpret, the patterns displayed by the instantaneous reaction rates with time are more complicated (Fig. 12). This is primarily the result of the fact that the reaction front, which is mostly clearly marked by the volume percentage of K-feldspar, is not stationary with time. As discussed in the introductory section on reaction-flow systems, the evolution of the mineral volume fractions and reactive surface areas cause the reaction path followed by the waters moving through the profile to change continuously. The instantaneous rate profile for K-feldspar, for example, develops a maximum about 4.5 m from the beginning of the flow path by 20,000 years due to the reduction in its reactive surface area over the first part of the profile. As the K-feldspar front migrates gradually downstream, its dissolution rate forms a traveling wave following the front. The downstream travel of the maximum in the K-feldspar dissolution rate causes a similar migration in the kaolinite precipitation rate, which is, of course, driven by K-feldspar dissolution. The traveling wave behavior displayed by the K-feldspar dissolution rate also explains the unusual pattern shown by the saturation index of kaolinite with time (Fig.

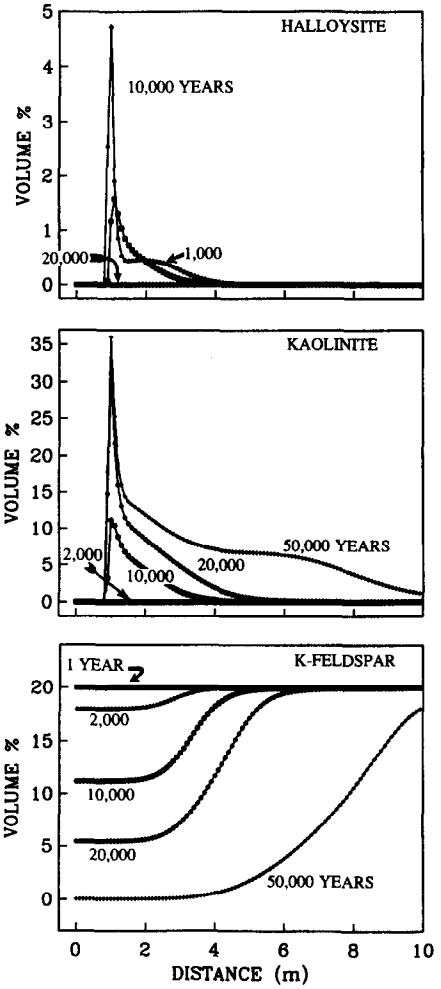

FIG. 11. Volume percentages of halloysite, kaolinite, and K-feldspar versus distance in the weathering profile. The halloysite volume fraction profile increases to a maximum by about 10,000 years, but disappears due to dissolution by 20,000 years. Note that the shape of the kaolinite profile is determined primarily by the initial halloysite nucleation event. The K-feldspar front migrates gradually downstream, so that by 50,000 years, K-feldspar is absent from the first 4 m of the profile.

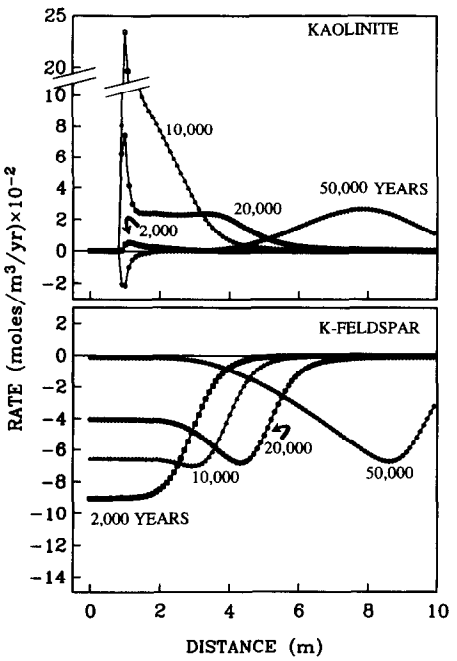

FIG. 12. Instantaneous reaction rates for kaolinite and K-feldspar. Negative and positive rates represent dissolution and precipitation, respectively. Note that the K-feldspar rate forms a wave which travels downstream. This is the result of the evolution of K-feldspar's volume fraction (and therefore, its reactive surface area) with time.

10c). As the K-feldspar front moves downstream into portions of the granite where the reactive surface area of kaolinite is lower (the profile of which is mostly determined by the initial nucleation event of halloysite), the saturation state of the waters with respect to kaolinite rises accordingly. By about 50,000 years, the waters 9 m from the beginning of the profile actually become supersaturated with respect to halloysite again (Fig. 10c), resulting in a second nucleation event (Fig. 10a). This kind of nonlinear phenomenon is primarily the result of the fact that a relatively short-lived nucleation event may determine the spatial distribution of secondary minerals, which in turn controls the chemical evolution of the waters moving through the rock.

It is worth noting that in the simulation presented, equilibrium with respect to kaolinite is never achieved for other than a brief time over a short distance along the flowpath. Close to the inlet, we see a decrease in the supersaturation of the solution with respect to kaolinite with time (1000, 10,000, and 20,000 a in Fig. 10c). However, by the time the solution reaches equilibrium with kaolinite, K-feldspar has completely disappeared from this portion of the flow path (Fig. 11). As a consequence, the solution becomes undersaturated with respect to kaolinite, and kaolinite begins to dissolve in this part of the profile (50,000 a in Fig. 10c). What the simulation shows is that partial equilibrium is the exception rather than the rule in low temperature water-rock systems. Where it appears, it results from the dynamic in-

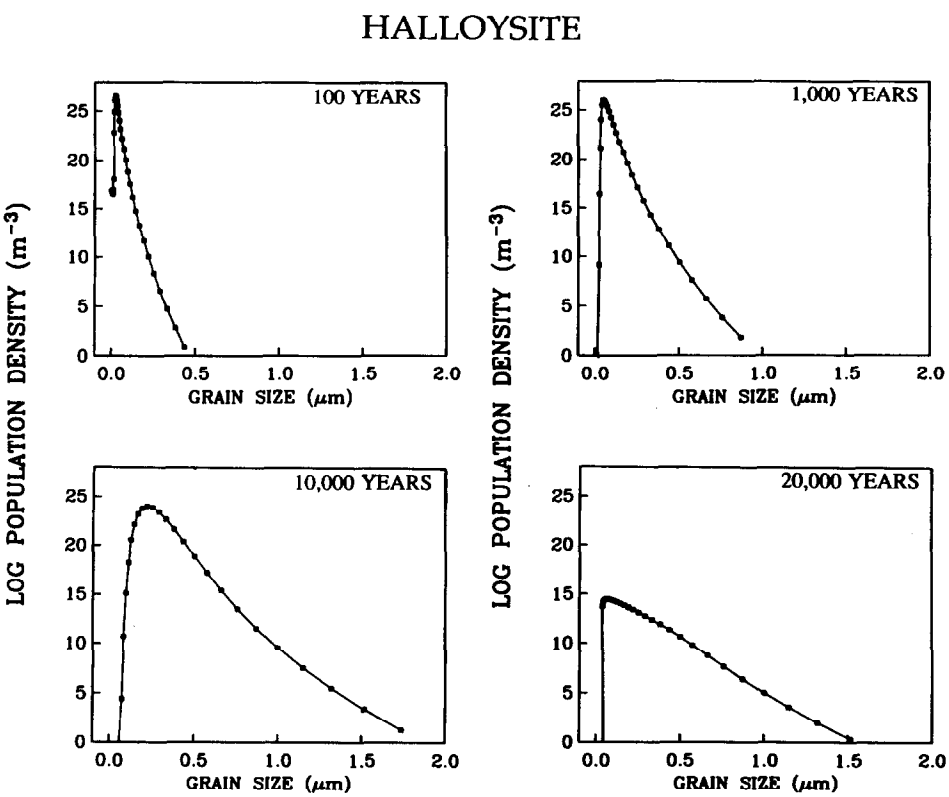

FIG. 13. Crystal size distribution (CSD) of halloysite 3 m from the inlet. Nucleation of halloysite crystallites is initially very rapid, but has ceased by 1000 years. Between 1000 and 10,000 years, the CSD of halloysite changes primarily due to Ostwald ripening, which because it causes larger crystals to grow at the expense of smaller ones, rotates the portion of the crystal size distribution at larger grain sizes to a shallower slope with time. By 20,000 years, dissolution has substantially reduced the number and size of halloysite crystals remaining.

terplay of simultaneous dissolution and precipitation reactions, as in the case of near-equilibrium with respect to halloysite in Fig. 8a.

Figure 13 shows the crystal size distribution for halloysite at 100, 1000, 10,000, and 20,000 years at a position 3 m from the top of the weathering profile. By 100 years, the nucleation rate has decreased from a maximum of about 10^{27} nuclei m^{-3} a^{-1} to about 10^{16} m^{-3} a^{-1} (indicated by the number of nuclei at the smallest grain size of 10 Å). By 1000 years, the halloysite nucleation event is over (at least at this particular point in space within the profile), as reflected by the movement of the crystal size distribution away from the 10 Å lower limit. The gradual rotation of the crystal size distribution at grain sizes larger than the maximum in population density is due to the effect of Ostwald ripening which accelerates the growth of the largest crystals in the system. By 20,000 years, the amplitude of the population density has decreased due to ripening, and the maximum in the population density has moved back to smaller grain sizes because of dissolution. The crystal size distribution of kaolinite forms a broadly similar pattern, except that it does not experience a dissolution event (Fig. 14). In this simulation, the generation of tiny kaolinite crystals occurs on the halloysite substrate, forming a distribution similar to what one would expect if kaolinite were nucleating directly. Shortly after 20,000 years, the production of tiny kaolinite crystallites ceases since the halloysite substrate is no longer present, and its crystal size distribution changes only due to crystal growth and Ostwald ripening. Note that most of the kaolinite crystals at 50,000 years are in the size range of about 1 to 20 microns, which agrees well with the range observed in natural settings. The range in crystal sizes predicted by the simulations, however, is sensitive to the form of the precipitation rate law which is used. If, for instance, m in Eqn. (8) is set equal to 1 instead of the value of 1/9 used in this simulation, the model predicts 300 micron kaolinite crystals within 500 years because of the high linear growth rates which result. This suggests that observations of the crystal size distribution of crystals may provide constraints on the actual precipitation rates of secondary minerals in natural environments.

CONCLUSIONS

The assumption of partial equilibrium with respect to secondary minerals in low temperature water-rock systems may not be justified in many instances. The common occurrence of metastable minerals and supersaturated solutions in surficial environments indicates that the production of reactive surface area of the thermodynamically most stable minerals may be a slow process. Much of the difficulty in creating reactive surface area can be attributed to low nucleation rates for such stable minerals as kaolinite. Nucleation is the most effective process by which new surface area is created, but it requires that the solution supersaturation exceeds some critical value. The more insoluble the mineral, the higher its interfacial tension with solution and the higher the required

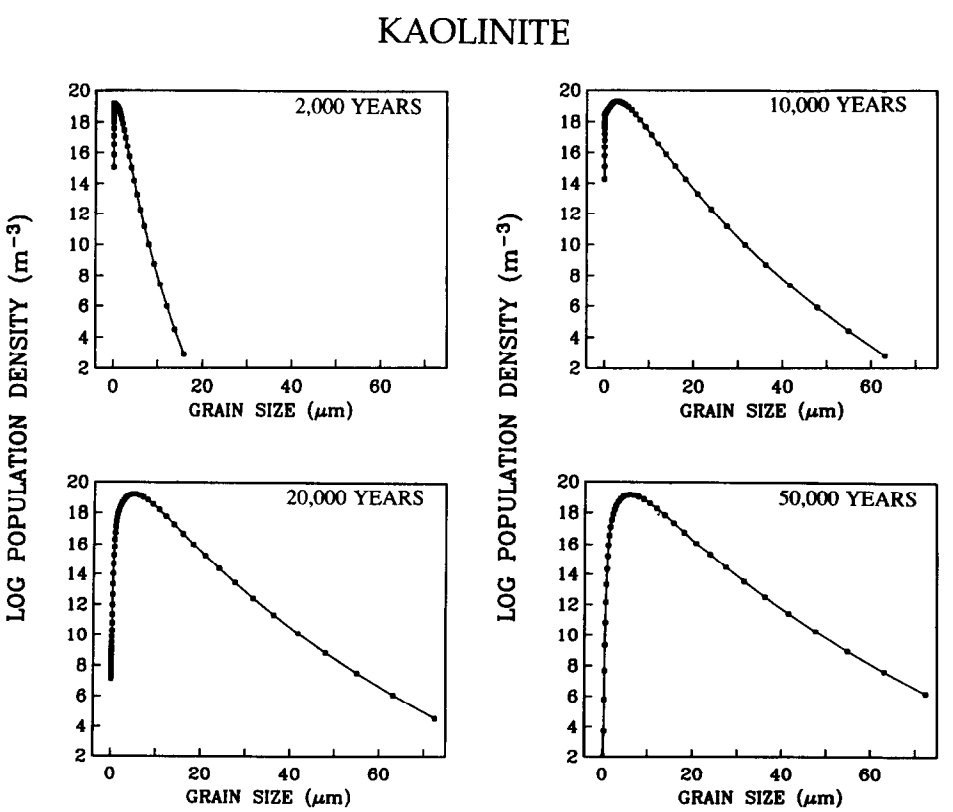

FIG. 14. Crystal size distribution for kaolinite 3 m from inlet. Once substantial amounts of halloysite have formed, the production of kaolinite crystals on the halloysite substrate is rapid. By 50,000 years, with the disappearance of halloysite, the CSD changes only due to crystal growth and Ostwald ripening.

critical supersaturation overstep. One way direct nucleation of a stable mineral may be circumvented is through the nucleation of a thermodynamically less stable precursor. The precursor can then be replaced by the stable mineral, either directly or through a series of intermediate phases. Observations of natural weathering profiles indicate that the process by which the precursor is converted to the stable phase may require geologically significant periods of time (GARRELS, 1982), as in the case of kaolinite (HEM et al., 1973). In this paper, we suggest that a kinetic approach to treating metastable precursors and their replacement by more stable minerals may be superior to the simple assumption of metastable equilibrium, because the kinetic approach is more general and yields information on the time scale of the aging process.

We have shown that it is possible to formulate a mathematical description of heterogeneous nucleation, growth and dissolution, Ostwald ripening, and precursor replacement, which gives at least a qualitatively correct description of the processes by which surface area is generated and modified. In addition, when combined with transport in a reactive flow scheme, the numerical simulations offer insights into how reaction fronts develop in space as well as time. A future application of this kind of approach would be to treat weathering as a quasi-steady state phenomenon in which the character of the profile is the result of the interplay of *all* the dynamic processes in the system, i.e., including erosion, rainfall, uplift, etc. If such models can be properly calibrated, they may provide a means of both interpreting paleo-weathering profiles and of estimating global chemical fluxes due to weathering in the past under conditions different from those of the present day. A completely rigorous model for water-rock interaction will require a great deal more experimental data on (and conceptual understanding of) mineral-aqueous solution interfacial tensions, crystal growth and dissolution rate laws, reaction pathways involving precursors, and ripening of crystal size distributions. However, we feel it is important to stress that despite their complexity, these processes must be understood if we are to obtain a truly quantitative understanding of water-rock interaction.

Acknowledgments—We thank Antonio Lasaga for providing various kinds of financial support to one of us (CIS) through grants from the National Science Foundation (grants EAR 8618307 and 8917056) and a departmental fellowship. He also kindly provided the Decstation 3100 which was used for the numerical simulations presented, and a good deal of the original inspiration to look at the problem of partial equilibrium in water-rock systems. One of us (PVC) was supported by the National Science Foundation Grant EAR 8617600 (R. A. Berner, P. I.). We are also indebted to Kathryn Nagy for a thorough review of the manuscript and numerous discussions on precipitation kinetics and to William Murphy with whom we had a discussion which provided much of the motivation for including surface area generation in a reactive flow model. We are grateful to two semi-anonymous *Geochimica* reviewers (DAC and JDR) and one anonymous reviewer for their constructive criticisms of the manuscript.

Editorial handling: E. J. Reardon

References

AAGAARD P. and HELGESON H. C. (1982) Thermodynamic and kinetic constraints on reaction rates among minerals and aqueous solutions, I, Theoretical considerations. *Amer. J. Sci.* **282**, 237–285.

ADAMSON A. W. (1982) *Physical Chemistry of Surfaces*. J. Wiley & sons.

ALEXANDER G. B., HESTON W. M., and ILER R. K. (1954) The solubility of amorphous silica in water. *J. Phys. Chem.* **58**, 453–455.

ANAND R. R., GILKES R. J., ARMITAGE T. M., and HILLYER J. W. (1985) Feldspar weathering in lateritic saprolite. *Clays Clay Mineral.* **33**, 31–43.

ARENDS J., CHRISTOFFERSEN J., CHRISTOFFERSEN M. R., ECKERT H., FOWLER B. O., HEUGHEBAERT J. C., NANCOLLAS G. H., YESINOWSKI J. P., and ZAWACKI S. J. (1987) A calcium hydroxyapatite precipitated from an aqueous solution. *J. Crystal. Growth* **84**, 512–532.

BALES R. C. and MORGAN J. J. (1985) Dissolution kinetics of chrysotile at pH 7 to 10. *Geochim. Cosmochim. Acta.* **49**, 2281–2288.

BARONNET A. (1982) Ostwald ripening in solution. The case of calcite and mica. *Estudios Geol.* **38**, 185–198.

BEAR J. (1979) *Hydraulics of Groundwater*. McGraw-Hill.

BERNER E. K. and BERNER R. A. (1987) *The Global Water Cycle*. Prentice-Hall.

BERNER R. A. (1970) Sedimentary pyrite formation. *Amer. J. Sci.* **268**, 1–23.

BERNER R. A. (1978) Rate control of mineral dissolution under earth surface conditions. *Amer. J. Sci.* **278**, 1235–1252.

BERNER R. A. (1980) *Early Diagenesis: A Theoretical Approach*. Princeton Univ. Press.

BERNER R. A. (1984) Sedimentary pyrite formation: An update. *Geochim. Cosmochim. Acta* **48**, 605–615.

BERNER R. A. and MORSE J. W. (1974) Dissolution kinetics of calcium carbonate in seawater: IV. Theory of calcite dissolution. *Amer. J. Sci.* **274**, 108–134.

BERNER R. A., WESTRICH J. T., GRABER R., SMITH J., and MARTENS C. S. (1978) Inhibition of aragonite precipitation from supersaturated seawater: A laboratory and field study. *Amer. J. Sci.* **278**, 816–837.

BLUM A. E. and LASAGA A. C. (1988) Role of surface speciation in the dissolution of minerals. *Nature* **331**, 341–343.

BOISTELLE R. (1982) Mineral crystallization from solution. *Estudios Geol.* **38**, 135–153.

BRADY P. V. and WALTHER J. V. (1989) Controls on silicate dissolution rates in neutral and basic pH solutions at 25°C. *Geochim. Cosmochim. Acta* **53**, 2823–2830.

BURTON E. A. and WALTER L. M. (1990) The role of pH in phosphate inhibition of calcite and aragonite precipitation rates in seawater. *Geochim. Cosmochim. Acta* **54**, 797–808.

BURTON W. K. and CABRERA N. (1949) Crystal growth and surface structure. *Disc. Faraday Soc.* **5**, 33–39.

BURTON W. K., CABRERA N., and FRANK F. C. (1951) The growth of crystals and the equilibrium structure of their surfaces. *Phil. Trans. Roy. Soc. London* **A243**, 299–358.

CARROLL-WEBB S. A. and WALTHER J. V. (1988) A surface complex reaction model for the pH-dependence of corundum and kaolinite dissolution rates. *Geochim. Cosmochim. Acta* **52**, 2609–2623.

CASEY W. H., WESTRICH H. R., and ARNOLD G. W. (1988) Surface chemistry of labradorite feldspar reacted with aqueous solutions at pH = 2, 3, and 12. *Geochim. Cosmochim. Acta* **52**, 2795–2807.

CHAI B. T. (1974) Mass transfer of calcite during hydrothermal recrystallization. In *Geochemical Transport and Kinetics* (eds. A. W. HOFFMANN et al.), pp. 205–218. Carnegie Inst., Washington.

CHAI B. T. (1975) The kinetics and mass transfer of calcite during hydrothermal recrystallization process. Ph.D dissertation, Yale Univ.

CHOU L. and WOLLAST R. (1984) Study of the weathering of albite at room temperature and pressure with a fluidized bed reactor. *Geochim. Cosmochim. Acta* **48**, 2205–2217.

CHRISTOFFERSEN J. (1980) Kinetics of dissolution of calcium hydroxyapatite. *J. Crystal. Growth* **49**, 29–44.

CHRISTOFFERSEN J. and CHRISTOFFERSEN M. R. (1984) Kinetics of dissolution of calcium hydroxyapatite. *Faraday Discuss. Chem. Soc.* **77**, 235–242.

CHRISTOFFERSEN J., CHRISTOFFERSEN M. R., KIBALCZYC W., and ANDERSEN F. A. (1989) A contribution to the understanding of the formation of calcium phosphates. *J. Crystal. Growth* **94,** 767–777.

CHURCHMAN G. J., and CARR R. M. (1975) The definition and nomenclature of halloysites. *Clays Clay Mineral.* **23,** 382–388.

CRERAR D. A., AXTMANN E. V., and AXTMANN R. C. (1981) Growth and ripening of silica polymers in aqueous solutions. *Geochim. Cosmochim. Acta* **45,** 1259–1266.

DOVE P. M. and CRERAR D. A. (1990) Kinetics of quartz dissolution in electrolyte solutions using a hydrothermal mixed flow reactor. *Geochim. Cosmochim. Acta* **54,** 955–969.

DUNNING W. J. (1969) General and theoretical introduction. In *Nucleation* (ed. A. C. ZETTLEMOYER), pp. 1–67. Marcel Dekker.

EBERL D. D., ŚRONDOŃ J., KRALIK M., TAYLOR B. E., and PETERMAN Z. E. (1990) Ostwald ripening of clays and metamorphic minerals. *Science* **248,** 474–477.

FETH J. H., ROBERSON C. E., and POLZER W. L. (1964) Sources of mineral constituents in water from granitic rocks, Sierra Nevada, California and Nevada. *USGS Water Supply Paper 1535-I.*

FRANKL D. R. and VENABLES J. A. (1970) Nucleation on substrates from the vapour phase. *Adv. Phys.* **19,** 409–456.

GARRELS R. M. (1982) Chemical equilibrium in sedimentary systems. *Estudios Geol.* **38,** 289–294.

GEBHARDT M. (1973) Epitaxy. In *Crystal Growth: An Introduction* (ed. P. HARTMAN), pp. 105–118. North-Holland Publ.

GIBBS J. W. (1928) *The Collected Works of J. Willard Gibbs, Volume I.* Longmans.

GRANDSTAFF D. W. (1977) Some kinetics of bronzite orthopyroxene dissolution. *Geochim. Cosmochim. Acta* **41,** 1097–1103.

GRANDSTAFF D. W. (1980) The dissolution rate of forsteritic olivine from Hawaiian beach sand. *3rd Intl. Symp. Water-rock Interaction,* Alberta Research Council, Edmonton, Alberta, Proceedings, 72–74.

HELGESON H. C. (1968) Evaluation of irreversible reactions in geochemical processes involving minerals and aqueous solutions—I. Thermodynamic relations. *Geochim. Cosmochim. Acta.* **32,** 853–877.

HELGESON H. C. (1979) Mass transfer among minerals and hydrothermal solutions. In *Geochemistry of Hydrothermal Ore Deposits* (ed. H. L. BARNES), pp. 568–610. J. Wiley & Sons.

HELGESON H. C., GARRELS R. M., and MACKENZIE F. T. (1969) Evaluation of irreversible reactions in geochemical processes involving minerals and aqueous solutions—II. Applications. *Geochim. Cosmochim. Acta* **33,** 455–482.

HELGESON H. C., MURPHY W. M., and AAGAARD P. (1984) Thermodynamic and kinetic constraints on reaction rates among minerals and aqueous solutions. II. Rate constants, effective surface area, and the hydrolysis of feldspar. *Geochim. Cosmochim. Acta* **48,** 2405–2432.

HEM J. D. and ROBERSON C. E. (1990) Aluminum hydrolysis reactions and products in mildly acidic aqueous systems. In *Chemical Modeling in Aqueous Systems II* (eds. D. C. MELCHIOR and R. L. BASSETT); *ACS Symp. Ser.* **416,** 429–446.

HEM J. D., ROBERSON C. E., LIND C. J., and POLZER W. L. (1973) Chemical interactions of aluminum with aqueous silica at 25°C. *USGS Water Supply Paper 1827-E.*

HOLDREN G. R., JR. and BERNER R. A. (1979) Mechanism of feldspar weathering. I. Experimental studies. *Geochim. Cosmochim. Acta* **43,** 1161–1171.

HOLDREN G. R., JR. and SPEYER P. M. (1985) Reaction rate-surface area relationships during the early stages of weathering—I. Initial observations. *Geochim. Cosmochim. Acta* **49,** 675–681.

INIGUEZ-RODRIGUEZ A. M. (1981) Basaltic and rhyolitic rocks as parent materials of halloysite on Argentine deposits. In *Int. Clay Conf. 1981* (eds. H. VAN OLPHEN and F. VENIALE), pp. 605–612. Elsevier.

INSKEEP W. P. and BLOOM P. R. (1985) An evaluation of rate equations for calcite precipitation kinetics at pCO_2 less than 0.01 atm and pH greater than 8. *Geochim. Cosmochim. Acta* **49,** 2165–2180.

INSKEEP W. P. and SILVERTOOTH J. C. (1988) Kinetics of hydroxyapatite precipitation at pH 7.4 to 8.4. *Geochim. Cosmochim. Acta* **52,** 1883–1893.

KIRKNER D. J. and REEVES H. (1988) Multicomponent mass transport with homogeneous and heterogeneous chemical reactions: Effect of chemistry on the choice of numerical algorithm. I. Theory. *Water Resources Res.* **24,** 1719–1729.

KITTRICK J. A. (1969) Soil minerals in the Al_2O_3–SiO_2– H_2O system and a theory of their formation. *Clays Clay Mineral.* **17,** 157–167.

KNAPP R. B. (1989) Spatial and temporal scales of local equilibrium in dynamic fluid-rock systems. *Geochim. Cosmochim. Acta* **53,** 1955–1964.

KNAUSS K. G. and WOLERY T. J. (1986) Dependence of albite dissolution kinetics on pH and time at 25°C and 70°. *Geochim. Cosmochim. Acta* **50,** 2481–2497.

KNAUSS K. G. and WOLERY T. J. (1987) The dissolution kinetics of quartz as a function of pH and time at 70°C. *Geochim. Cosmochim. Acta* **52,** 43–53.

KNAUSS K. G. and WOLERY T. J. (1989) Muscovite dissolution kinetics as a function of pH and time at 70°C. *Geochim. Cosmochim. Acta* **53,** 1493–1501.

KRONBERG B. I., TAZAKI K., and MELFI A. J. (1987) Detailed geochemical studies of the initial stages of weathering of alkaline rocks: Ilha de Sao Sebastiao, Brazil. *Chem. Geol.* **60,** 79–88.

LANGMUIR D. (1971) Particle size effect on the reaction goethite = hematite + water. *Amer. J. Sci.* **271,** 147–156.

LANGMUIR D. and WHITTEMORE D. O. (1971) Variations in the stability of precipitated ferric oxy-hydroxides. In *Nonequilibrium Systems in Natural Water Chemistry* (ed. R. F. GOULD); *ACS Symp. Ser. 106,* pp. 209–234.

LASAGA A. C. (1984) Chemical kinetics of water-rock interactions. *J. Geophys. Res.* **89,** 4009–4025.

LICHTNER P. C. (1985) Continuum model for simultaneous chemical reactions and mass transport in hydrothermal systems. *Geochim. Cosmochim. Acta* **49,** 779–800.

LICHTNER P. C. (1988a) The quasi-stationary state approximation to coupled mass transport and fluid-rock interaction in a porous medium. *Geochim. Cosmochim. Acta* **52,** 143–165.

LICHTNER P. C. (1988b) Multiple reaction path model describing mass transfer in geochemical systems. In *Proceedings of the Workshop on Geochemical Modeling* (compiled by K. J. JACKSON and W. L. BOURCIER), pp. 3–9. Lawrence Livermore Natl. Lab.

LIFSHITZ I. M. and SLYOZOV U. V. (1961) The kinetics of precipitation from supersaturated solid solutions. *J. Phys. Chem. Solids* **19,** 35–50.

LIN F. and CLEMENCY C. V. (1981) The kinetics of dissolution of muscovite at 25°C and 1 atm CO_2 partial pressure. *Geochim. Cosmochim. Acta* **45,** 571–576.

LOTHE J. and POUND G. M. (1966) On the statistical mechanics of nucleation theory. *J. Chem. Phys.* **45,** 630–634.

MADÉ B. and FRITZ B. (1989) Simulation of granite dissolution at 25, 60 and 100°C based on thermodynamic potential and kinetic laws. In *Water-Rock Interaction* (ed. D. L. MILES), pp. 461–464. Balkema, Rotterdam.

MARQUSEE J. A. and ROSS J. (1983) Kinetics of phase transitions: theory of Ostwald ripening. *J. Chem. Phys.* **79,** 373–378.

MCDONALD J. E. (1962) Homogeneous nucleation of vapor condensation. I. Thermodynamic aspects. *Amer. J. Phys.* **30,** 870–877.

MORSE J. W. and CASEY W. H. (1988) Ostwald processes and mineral paragenesis in sediments. *Amer. J. Sci.* **288,** 537–560.

MURPHY W. M. and HELGESON H. C. (1989) Thermodynamic and kinetic constraints on reaction rates among minerals and aqueous solutions. IV. Retrieval of rate constants and activation parameters for the hydrolysis of pyroxene, wollastonite, olivine, andalusite, quartz, and nepheline. *Amer. J. Sci.* **289,** 17–101.

NAGY K. L., BLUM A. E., and LASAGA A. C. (1988) Precipitation kinetics and solubility of kaolinite in dilute aqueous solutions at 80°C. *GSA Abstr. with Prog.,* A42.

NAGY K. L., STEEFEL C. I., BLUM A. E., and LASAGA A. C. (1990) Dissolution and precipitation kinetics of kaolinite: initial results at 80°C with application to porosity evolution in a sandstone. *AAPG Spec. Publ.* (in press).

NANCOLLAS G. H. and PURDIE N. (1964) The kinetics of crystal growth. *Qtly. Rev. Chem. Soc.* **18,** 1–20.

NANCOLLAS G. H. and REDDY M. M. (1971) The crystallization of calcium carbonate II. Calcite growth mechanisms. *J. Colloid Interface Sci.* **36,** 166–172.

NESTAAS I. and TERJESEN S. G. (1969) The inhibiting effect of scandium ions upon the dissolution of calcium carbonate. *Acta Chemica Scandinavica* **23,** 2519–2531.

NIELSEN A. E. (1964) *The Kinetics of Precipitation.* MacMillan.

NIELSEN A. E. (1982) Theory of electrolyte crystal growth. In *Industrial Crystallization* (eds. S. J. JANČIC and E. J. DE JONG), pp. 35–44. North-Holland Publ. Co.

NIELSEN A. E. (1984) Electrolyte crystal growth mechanisms. *J. Crystal Growth* **67,** 289–310.

NIELSEN A. E. (1986) Mechanisms and rate laws in electrolyte crystal growth from aqueous solution. In *Geochemical Processes at Mineral Surfaces* (ed. J. A. DAVIS and K. F. HAYES); *ACS Symp. Ser. 323,* pp. 600–614.

NIELSEN A. E. and CHRISTOFFERSEN J. (1982) The mechanisms of crystal growth and dissolution. In *Biological Mineralization and Demineralization* (ed. G. H. NANCOLLAS), pp. 37–77. Springer-Verlag.

NIELSEN A. E. and SÖHNEL O. (1971) Interfacial tensions electrolyte crystal-aqueous solutions, from nucleation data. *J. Crystal. Growth* **11,** 233–242.

NIELSEN A. E. and TOFT J. M. (1984) Electrolyte crystal growth kinetics. *J. Crystal. Growth* **67,** 278–288.

OHARA M. and REID R. C. (1973) *Modeling Crystal Growth Rates from Solution.* Prentice-Hall.

ORTOLEVA P., CHADAM J., MERINO E., and SEN A. (1987) Geochemical self-organization II: The reactive-infiltration instability. *Amer. J. Sci.* **287,** 1008–1040.

PAČES T. (1978) Reversible control of aqueous aluminum and silica during the irreversible evolution of natural waters. *Geochim. Cosmochim. Acta* **42,** 1487–1493.

PARHAM W. E. (1969a) Halloysite-rich tropical weathering products of Hong Kong. *Proc. Intl. Clay Conf. 1969.* **I,** 403–416.

PARHAM W. E. (1969b) Formation of halloysite from feldspar: Low temperature artificial weathering versus natural weathering. *Clays Clay Mineral.* **17,** 13–22.

PARKS G. A. (1984) Surface and interfacial free energies of quartz. *J. Geophys. Res.* **89,** 3997–4008.

PHELAN P. J. and MATTIGOD S. V. (1987) Kinetics of heterogeneously initiated precipitation of calcium phosphates. *Soil Sci. Soc. Amer. J.* **51,** 336–341.

PLUMMER L. N., WIGLEY T. M. L., and PARKHURST D. L. (1979) Critical review of the kinetics of calcite dissolution and precipitation. In *Chemical Modeling in Aqueous Systems I*(ed. E. A. JENNE); *ACS Symp. Ser. 93,* pp. 537–573.

POUND G. M., SIMNAD M. T., and YANG L. (1954) Heterogeneous nucleation of crystals from vapor. *J. Chem. Phys.* **22,** 1215–1219.

PRESS W. H., FLANNERY B. P., TEUKOLSKY S. A., and VETTERLING W. T. (1986) *Numerical Recipes: The Art of Scientific Computing.* Cambridge, Cambridge University Press.

RANDOLPH A. D. and LARSON M. A. (1988) *Theory of Particulate Processes.* Academic Press.

RAYMAHASHAY B. C., RAO K. S., MEHTA V. K., and BHAVANA P. R. (1987) Mineralogy and geochemistry of lateritic soil profiles in Kerola, India. *Chem. Geol.* **60,** 327–330.

REDDY M. M. (1986) Effect of magnesium ions on calcium carbonate nucleation and crystal growth in dilute aqueous solutions at 25°C. In *Studies in Diagenesis* (ed. F. A. MUMPTON); *USGS Bull. 1578,* pp. 169–182.

REED M. H. (1982) Calculation of multicomponent chemical equilibria and reaction processes in systems involving minerals, gases, and an aqueous phase. *Geochim. Cosmochim. Acta* **46,** 513–528.

REEVES H. and KIRKNER D. J. (1988) Multicomponent mass transport with homogeneous and heterogeneous chemical reactions: Effect of chemistry on the choice of numerical algorithm. 2. Numerical results. *Water Resources Res.* **24,** 1730–1739.

RENDERS P. J. N. and BARNES H. L. (1989) Hydrothermal precipitation of cristobalite at 200°C. *Geol. Soc. Amer. Abst. Prog. 1989,* A103.

RIMSTIDT J. D. and BARNES H. L. (1980) The kinetics of silica-water reactions. *Geochim. Cosmochim. Acta* **44,** 1683–1699.

SALTER T. L. and MURRAY H. H. (1989) Morphology of halloysite in a laterite from Saline County, Arkansas, U.S.A. *9th Intl. Clay Conf. Abstr., June 1989,* 335.

SAYLES F. L. and FYFE W. S. (1973) The crystallization of magnesite from aqueous solution. *Geochim. Cosmochim. Acta* **37,** 87–99.

SCHENK D., PETERSEN A., and MATTHESS G. (1989) Acceleration and retardation of silicate weathering due to organic substances. In *Water-Rock Interaction* (ed. D. L. MILES), pp. 605–607. Balkema, Rotterdam.

SCHINDLER P. W. (1967) Heterogeneous equilibria involving oxides, hydroxides, carbonates, and hydroxide carbonates. In *Equilibrium Concepts in Natural Water Systems* (ed. W. STUMM); *ACS Symp. Ser. 67,* pp. 196–221.

SCHOTT J., and BERNER R. A. (1983) X-ray photoelectron studies of the mechanism of iron silicate dissolution during weathering. *Geochim. Cosmochim. Acta* **47,** 2233–2240.

SCHOTT J. and BERNER R. A. (1985) Dissolution mechanisms of pyroxenes and olivines during weathering. In *Chemistry of Weathering* (ed. J. I. DREVER), pp. 35–53. D. Reidel Publ. Co.

SCHOTT J. and PETIT J-C. (1987) New evidence for the mechanisms of dissolution of silicate minerals. In *Aquatic Surface Chemistry* (ed. W. STUMM), pp. 293–312. J. Wiley & Sons.

SCHOTT J., BERNER R. A., and SJÖBERG E. L. (1981) Mechanism of pyroxene and amphibole weathering—I. Experimental studies of iron-free minerals. *Geochim. Cosmochim. Acta* **45,** 2123–2135.

SIEFFERMANN G. and MILLOT G. (1969) Equatorial and tropical weathering of recent basalts from Cameroon: Allophanes, halloysite, metahalloysite, kaolinite, and gibbsite. *Proc. Intl. Clay Conf. 1969* **I,** 417–430.

SIEVER R. (1957) The silica budget in the sedimentary cycle. *Amer. Mineral.* **42,** 821–841.

SJÖBERG E. L. (1978) Kinetics and mechanism of calcite dissolution in aqueous solutions at low temperatures. *Stockholm Contrib. Geol.* **32.**

SMITH R. W. and HEM J. D. (1972) Effect of aging on aluminum hydroxide complexes in dilute aqueous solutions. *USGS Water Supply Paper 1827-D.*

STEEFEL C. I. and LASAGA A. C. (1990) Evolution of dissolution patterns: Permeability change due to coupled flow and reaction. In *Chemical Modeling in Aqueous Systems II* (ed. D. C. MELCHIOR and R. L. BASSETT); *ACS Symp. Ser. 416,* pp. 212–225.

STOER J. and BULIRSCH R. (1980) *Introduction to Numerical Analysis.* Springer-Verlag.

STUMM W. and MORGAN J. J. (1981) *Aquatic Chemistry: An Introduction Emphasizing Chemical Equilibria in Natural Waters.* J. Wiley & Sons.

TOSCHEV S. (1973) Homogeneous nucleation. In *Crystal Growth: An Introduction* (ed. P. HARTMAN), pp. 1–49. North-Holland Publ.

TSUZUKI Y. and KAWABE I. (1983) Polymorphic transformations of kaolin minerals in aqueous solutions. *Geochim. Cosmochim. Acta* **47,** 59–66.

TURNBULL D. (1950) Isothermal rate of solidification of small droplets of mercury and tin. *J. Chem. Phys.* **18,** 768–769.

VAN CAPPELLEN P. (1990) The formation of marine apatite: A kinetic study. Ph.D dissertation, Yale Univ.

VAN CAPPELLEN P. and BERNER R. A. (1989) Marine apatite precipitation. In *Water-Rock Interaction* (ed. D. L. MILES), pp. 707–710. Balkema, Rotterdam.

VAN CAPPELLEN P. and BERNER R. A. (1990) Fluorapatite crystal growth from artificial seawater solutions. *Geochim. Cosmochim. Acta* (submitted).

VAN DER MERWE J. H. and BALL C. A. B. (1975) Energy of interfaces between crystals. In *Epitaxial Growth Part B* (ed. J. W. MATTHEWS), pp. 493–528. Academic Press.

VOLMER M. (1945) *Kinetik der Phasenbildung.* Edwards Brothers.

WAGNER C. (1961) Theorie der Alterung von Niederschlägen durch Umlösen. *Ber. Bunsenges. Phys. Chem.* **651,** 581–591.

WALTON A. G. (1967) *The Formation and Properties of Precipitates.* Interscience Publ.

WHITE A. F. and PETERSON M. L. (1990) Role of reactive-surface area characterization in geochemical kinetic models. In *Chemical Modeling in Aqueous Systems II; ACS Symp. Series 416*, pp. 461–475.

WIELAND E., WEHRLI B., and STUMM W. (1988) The coordination chemistry of weathering: III. A generalization on the dissolution rates of minerals. *Geochim. Cosmochim. Acta* **52**, 1969–1981.

WOLERY T. J. (1979) Calculation of chemical equilibrium between aqueous solutions and minerals: The EQ3/EQ6 software package. UCRL-52658.

WOLERY T. J. (1983) EQ3NR, a computer program for geochemical aqueous speciation-solubility calculations: Users guide and documentation. *Lawrence Livermore Laboratory URCL-53414.*

WOLLAST R. (1967) Kinetics of the alteration of K-feldspar in buffered solutions at low temperature. *Geochim. Cosmochim. Acta* **31**, 635–648.

WOLLAST R. and CHOU L. (1985) Kinetic study of the dissolution of albite with a continuous flow-through fluidized bed reactor. In *The Chemistry of Weathering* (ed. J. I. DREVER), pp. 75–91. D. Reidel.

ZAWACKI S. J., KOUTSOUKOS P. B., SALIMI M. H., and NANCOLLAS G. H. (1986) The growth of calcium phosphates. In *Geochemical Processes at Mineral Surfaces* (ed. J. A. DAVIS and K. F. HAYES); *ACS Symp. Ser. 323*, pp. 650–662.

Appendix I: Numerical Computation of Reaction-Transport

The simulations of reactive flow are carried out by numerically solving for Eqn. (3) in one dimension. The partial differential equations for multi-component reaction and transport are converted into a set of algebraic equations using standard finite-difference methods, although the presence of the nonlinear reaction terms require that non-standard means of solving the PDEs be implemented. A modified Newton method is used which solves a fully coupled set of N_cM equations at every iteration, where M is the number of grid points in the system and N_c is the number of linearly independent chemical components in the system (KIRKNER and REEVES, 1988). The N_c linearly independent components are also referred to as basis components (e.g., WOLERY, 1983) or primary species (LICHTNER, 1985). These components completely describe the solution composition of the system.

The "secondary species," x_i can be written in terms of the basis components, c_j. If equilibrium between secondary species and basis components is assumed, then

$$x_i = \gamma_i^{-1} K_i \prod_{j=1}^{N_c} a_j^{\nu_{ij}} \quad (i = 1, \ldots, N_x) \tag{I-1}$$

where N_x is the number of secondary species in the system, ν_{ij} are the stoichiometric coefficients for the homogeneous reaction, K_i is the equilibrium constant, a_j are the activities of the primary species, and γ_i is the activity coefficient of the secondary species. These mass action expressions allow us to define a total component concentration (REED, 1982; LICHTNER, 1985; KIRKNER and REEVES, 1988)

$$u_j = c_j + \sum_{i=1}^{N_x} \nu_{ij} x_i, \tag{I-2}$$

or, using Eqn. (I-1),

$$u_j = c_j + \sum_{i=1}^{N_x} \nu_{ij} \gamma_i^{-1} K_i \prod_{j=1}^{N_c} a_j^{\nu_{ij}}. \tag{I-3}$$

Using Al as an example, if Al^{3+} is the basis species and for simplicity $Al(OH)^{2+}$ is the only secondary species, then

$$\begin{aligned} u_{Al^{3+}} &= (c_{Al^{3+}} + c_{Al(OH)^{2+}}) \\ &= c_{Al^{3+}} + \frac{K_{Al(OH)^{2+}} a_{Al^{+3}}}{a_{H+}} \gamma_{Al(OH)^{2+}}^{-1}. \end{aligned} \tag{I-4}$$

As noted by REED (1982) and LICHTNER (1985), in the case of H^+ and redox species, there is no simple physical meaning to the "total concentration" since these concentrations may be negative.

Following the notation of KIRKNER and REEVES (1988), we can introduce a convection-dispersion spatial operator

$$L(u_j) = \nabla \cdot [(u_j)\mathbf{q} - \phi \mathbf{D} \nabla (u_j)] \tag{I-5}$$

where $\mathbf{q}$ is the Darcian flux and $\mathbf{D}$ is the combined dispersion-diffusion coefficient. The governing differential equations can then be written in terms of the total component concentrations as

$$\frac{\partial}{\partial t}(\phi u_j) + L(u_j) + R(c_1, \ldots, c_{Nc}) = 0 \tag{I-6}$$

where the heterogeneous reaction term R affecting the total concentration u_j is expressed as a function of the primary species in the system. This formulation works without modification when the dispersion-diffusion coefficients for all of the species (primary and secondary) are assumed to be the same and when the reactions are electrically balanced (LICHTNER, 1985).

In our benchmark tests we have found (as did REEVES and KIRKNER, 1988) that the most robust solution method directly couples the speciation calculations to the differential equations. Substituting Eqn. (I-3) into Eqn. (I-6), we obtain

$$\left(\frac{\partial \phi}{\partial t} + L\right)\left[c_j + \sum_{i=1}^{N_x} \nu_{ij} \gamma_i^{-1} K_i \prod_{j=1}^{N_c} a_j^{\nu_{ij}}\right] + R(c_1, \ldots, c_{Nc}) = 0 \tag{I-7}$$

which allows us to limit the number of differential equations which must be solved at each grid point to the number of basis components in the system, N_c. By solving directly for the individual components, the heterogeneous reaction terms and the speciation calculations, which are functions of the c_j's, are directly coupled in the Newton iterations.

The system of equations which result from the finite difference approximation of Eqn. (I-7) forms a sparse matrix since the chemical components at the nth grid point are linked only to the two adjacent grid points. The block tridiagonal form of the Jacobian matrices, in which the N_c by N_c submatrices arise from the coupling of the components involved in the homogeneous and heterogeneous reactions, suggest the use of block iterative methods which automatically take full advantage of the sparseness of the finite difference formulations (STOER and BULIRSCH, 1980; PRESS et al., 1986). The block iterative methods are particularly useful for reaction-transport problems in that the dense diagonal submatrix containing the homogeneous and heterogeneous reaction contributions can be inverted directly and efficiently by standard methods (e.g., LU decomposition), thus reducing the total number of iterations required.

Another important feature which we have incorporated into our numerical scheme is automatic basis switching. Basis switching consists of choosing the dominant species at any point within a flow field as the primary species or basis component. As discussed by WOLERY (1983), basis switching greatly improves the numerical stability of the Newton scheme. In using basis switching in a finite difference formulation, however, an additional procedure is needed to correct the fluxes between two adjacent grid points that are using different basis sets.

Appendix II: Heterogeneous Nucleation

Heterogeneous nucleation from aqueous solution results from the movement and association as small clusters of ions adsorbed at the surface of a solid substrate. When the bulk solution is supersaturated, there is a finite probability that some of the clusters attain the critical size and continue to grow into crystals of the new solid phase. The energetics of heterogeneous nucleation are governed by the free energy of formation of the clusters,

$$\Delta G(n) = -nk_bT \ln \Omega + \Delta G_{ex}(n) \tag{II-1}$$

where n is the number of formula units of mineral in the cluster, Ω is the saturation index (Eqn. 7 in text), and ΔG_{ex} is the excess amount of energy required to form the surface of the cluster.

In the model, we assume that upon formation of a cluster, the interfacial work results primarily from the creation of additional solid-solution interface (VAN CAPPELLEN, 1990), or,

$$\Delta G_{ex} \approx (A_{cw} - A_{cs})\sigma_{cw} \quad \text{(II-2)}$$

where A is the interfacial area, σ is the interfacial free energy per unit area, and the subscripts stand for cw = cluster-water and cs = cluster-substrate. In other words, the nucleating mineral selects the most suitable substrate in order to minimize the cluster-substrate interfacial free energy. This is probably not unreasonable for a natural water-rock system in which there is a variety of substrate surfaces to choose from. To calculate Eqn. (II-2) explicitly, a geometry has to be assigned to the clusters. For simplicity, we assume that the clusters are half spheres on a planar substrate, and Eqn. (II-2) becomes

$$\Delta G_{ex}(n) = \pi r^2\sigma = \pi^{1/3}\left(\frac{3v}{2}\right)^{2/3} n^{2/3}\sigma \quad \text{(II-3)}$$

where r is the radius of the cluster and v is the volume of a formula unit of mineral ($v = 2\pi r^3/3n$). For convenience, we have omitted the subscript from the mineral-water interfacial tension of the nucleating mineral.

Equations (II-1) and (II-3) can be combined, and by solving for $d\Delta G/dn = 0$, we find the size of the critical nucleus:

$$n^* = \frac{2\pi v^2\sigma^3}{3(k_bT \ln \Omega)^3} \quad \text{(II-4)}$$

from which we derive the radius of the critical nucleus,

$$r^* = \frac{v\sigma}{k_bT \ln \Omega} \quad \text{(II-5)}$$

and its free energy of formation,

$$\Delta G^* = \frac{\pi v^2\sigma^3}{3(k_bT \ln \Omega)^2}. \quad \text{(II-6)}$$

The classical theory of nucleation assumes that when an additional growth unit is attached to a cluster of critical dimension, the latter will grow irreversibly to macroscopic dimensions. Thus, the rate of nucleation is given by product of the concentration of critical nuclei times the frequency of successful attachment of an ion to a nucleus. The concentration of critical nuclei is assumed to satisfy a simple equilibrium distribution:

$$N^* = N_{ad} \exp(-\Delta G^*/k_bT) \quad \text{(II-7)}$$

where N^* is the number of critical nuclei per unit substrate surface (= surface density) and N_{ad} is the mean surface density of growth units of the nucleating mineral in the adsorption layer on the substrate. Assuming equilibrium between the adsorption layer and the bulk solution, we have (NIELSEN, 1984, 1986)

$$N_{ad} = K_{ad}CaL \quad \text{(II-8)}$$

where K_{ad} is the dimensionless equilibrium adsorption constant, C is the mean concentration of the mineral in the bulk solution, a is the mean ionic diameter (we use 3 Å), and L is Avogadro's number. The mean concentration in solution of a mineral ($A_\alpha B_\beta \cdots$) is given by

$$C \approx C_{sat}\Omega^{1/\eta} \quad \text{(II-9)}$$

where η is the number of ions per formula unit mineral ($\eta = \alpha + \beta + \cdots$). The adsorption constant K_{ad} depends on both the adsorbate and the adsorbent surface. For adsorption of aqueous ions on mineral surfaces at 25°C, the range of K_{ad} should be similar to that found for the adsorption constants of electrolytes on their corresponding crystals, 10 to 10^3 (NIELSEN, 1984, 1986). In the simulations we use a representative value, $K_{ad} = 100$.

The structural sites at which growth units are added to the nucleus are described as kink sites (BURTON and CABRERA, 1949; BURTON et al., 1951). If x_o is the mean distance between two kinks, then the number of kinks along the edge of the critical nucleus is $2\pi r^*/x_o$. The mean distance x_o is given by (NIELSEN, 1984)

$$x_o = \frac{a \exp(a^2\sigma/k_bT)}{\Omega^{1/2\eta}}. \quad \text{(II-10)}$$

Assuming that the integration at the kink sites is the rate-limiting step for the growth of a nucleus, the nucleation rate will be determined by the frequency, f, at which ions enter a kink (NIELSEN, 1984),

$$f = 2\nu_{in}P_{ad} \quad \text{(II-11)}$$

where ν_{in} is the jumping frequency for an adsorbed ion into a kink site and P_{ad} is the probability that an adsorption site next to a kink is actually occupied by an ion. The "2" in front of the right-hand side of Eqn. (II-11) corresponds to the two adsorption sites adjacent to a kink for a simple cubic structure of kinks and growth units. The occupancy probability P_{ad} for simple monolayer adsorption is estimated as

$$P_{ad} = a^2N_{ad} \quad \text{(II-12)}$$

where we assume that the total number of ionic adsorption sites per unit surface area may be approximated by $1/a^2$. The jump frequency ν_{in} is related to the fundamental frequency, $\nu_o = k_bT/h$, by

$$\nu_{in} = \nu_o \exp(-G_a/k_bT) \quad \text{(II-13)}$$

where G_a is the Gibbs activation free energy for the integration of an ion into a kink site. Values of G_a range from 30 to 120 kJ/mol (e.g., NIELSEN, 1982; NIELSEN and CHRISTOFFERSEN, 1982). In the simulations we use G_a = 71 kJ/mol for all the nucleating minerals, except for gibbsite, which we assign a value of 100 kJ/mol based on the high Arrhenius activation energy for precipitation of aluminum hydroxide (HEM and ROBERSON, 1990).

Finally, the steady-state rate of heterogeneous nucleation, J, can be calculated as

$$J = A_sfN^*\left(\frac{2\pi r^*}{x_o}\right) \quad \text{(II-14)}$$

where A_s is the area of substrate per unit volume total rock and J is expressed in nuclei per unit time per unit volume rock. By combining Eqn. (II-5) with Eqns. (II-7) to (II-13), Eqn. (II-14) can be rewritten as

$$J = J_o \exp(-\Delta G^*/k_bT) \quad \text{(II-15)}$$

with the pre-exponential factor J_o given by

$$J_o = 4\pi A_s\nu_o\sigma(K_{ad}C_{sat}a^2L)^2\left(\frac{\Omega^{5/2\eta}}{\ln \Omega}\right)\left(\frac{a^2\sigma}{k_bT}\right) \times \exp(-\sigma a^2/k_bT)\exp(-G_a/k_bT) \quad \text{(II-16)}$$

where C_{sat} is the solubility of the mineral. By definition, C_{sat} is the number of moles of formula units of mineral dissolving in pure water to saturation.

Appendix III: Surface Cannibalism

In the model, kaolinite surface area is created by direct heterogeneous nucleation of kaolinite from solution, through crystal growth on existing kaolinite surface area, and through "cannibalism" of the precursor's surface area. In the latter process, kaolinite and the precursor (halloysite) compete for available growth sites on the surface of the precursor. Let $\rho_{s,\text{tot}}$ be the total density of growth sites on the surface of the precursor. The number of growth sites per unit surface area which continue to grow as kaolinite rather than halloysite is given by

$$\rho_{s,\text{kaol}} = P\rho_{s,\text{tot}} \quad \text{(III-1)}$$

where P is the probability that a given surface growth site on halloysite decides to grow as kaolinite. We assume that the probability P follows Boltzmann's distribution law,

$$P = \exp(-\Delta G_{s,\text{kaol}}/k_bT) \qquad \text{(III-2)}$$

where $\Delta G_{s,\text{kaol}}$ is the free energy needed to create a kaolinite growth center out of a halloysite kink site. The formation of a kaolinite growth center is opposed by the higher mineral-water interfacial tension of kaolinite relative to that of the precursor, but promoted by kaolinite's lower solubility. Neglecting the interfacial tension between the precursor and kaolinite on the basis of the chemical and structural similarity,we may write

$$\Delta G_{s,\text{kaol}} = b_1a^2(\sigma_{\text{kaol}} - \sigma_{\text{hall}}) + b_2k_bT \ln\left(\frac{K_{\text{kaol}}}{K_{\text{hall}}}\right)^{1/9} \qquad \text{(III-3)}$$

where σ_i is the mineral-water interfacial free energy, K_i is the solubility product, a is the molecular length scale (Appendix II), and the subscripts kaol and hall stand for kaolinite and halloysite respectively. The constants b_1 and b_2 are related to the effective number of structural units per growth center and their geometry. If we take a simple cubic geometry for kinks and growth units, the minimum requirement to change a kink site on the surface of the precursor into a growth center for kaolinite is to replace the three structural units forming the three sides of the kink by three kaolinite units; hence, $b_1 = 6$ and $b_2 = 3$. At 25°C, for a range of $\sigma_{\text{kaol}} - \sigma_{\text{hall}}$ from 100 to 150 mJ/m^2, the probability ranges from 10^{-7} to 10^{-10}. Because of the low values of P and, thus, the slow rate of surface cannibalism, the precursor can persist over significant periods of time before it is replaced by the stable mineral (see Fig. 8 and 9). The probability of forming a critical nucleus of kaolinite under the same conditions (i.e., by direct heterogeneous nucleation), however, is only on the order of 10^{-24}, making precipitation via the precursor the preferred pathway for the formation of kaolinite.